SpezialForschungsBereich F 32

Karl–Franzens Universität Graz
Technische Universität Graz
Medizinische Universität Graz

A flexible space-time discontinuous Galerkin method for parabolic initial boundary value problems

M. Neumüller O. Steinbach

SFB-Report No. 2011-013 June 2011

A–8010 GRAZ, HEINRICHSTRASSE 36, AUSTRIA

Supported by the
Austrian Science Fund (FWF)

Der Wissenschaftsfonds.

SFB sponsors:

- **Austrian Science Fund** (FWF)
- **University of Graz**
- **Graz University of Technology**
- **Medical University of Graz**
- **Government of Styria**
- **City of Graz**

A flexible space–time discontinuous Galerkin method for parabolic initial boundary value problems

M. Neumüller, O. Steinbach

Institut für Numerische Mathematik, TU Graz,
Steyrergasse 30, 8010 Graz, Austria
{neumueller, o.steinbach}@tugraz.at

Abstract

In this paper we present a discontinuous Galerkin finite element method for the solution of parabolic initial boundary value problems. The approach is based on a decomposition of the space–time cylinder into finite elements, which also allows a rather general and flexible discretization in time. This also includes adaptive finite element meshes which move in time. For the handling of three–dimensional spatial domains, and therefore of a four–dimensional space–time cylinder, we describe a refinement strategy to decompose pentatopes into smaller ones. For the discretization of the initial boundary value problem we use an interior penalty Galerkin approach in space, and an upwind technique in time. A numerical example for the transient heat equation confirms the order of convergence as expected from the theory. First numerical results for the transient Navier–Stokes equations and for an adaptive mesh moving in time underline the applicability and flexibility of the presented approach.

1 Introduction

The finite element approximation of transient partial differential equations is in most cases based on explicit or implicit time discretization schemes. In particular the simultaneous consideration of different time steps requires an appropriate interpolation to couple the solutions at different time levels. Instead, in this paper we consider the application of finite elements in the space–time cylinder.

Space–time finite element methods have been applied to several parabolic model problems. Least square methods for convection–diffusion problems are considered, e.g., in [5], and for flow problems, e.g., in [15, 20, 21, 22, 23]. Discontinuous Galerkin finite element methods have been applied to solve transient problems for advection–diffusion problems in [19], and for flow problems in [7, 25]. In most cases, the time dependent equation is discretized in the space–time domain or on so called space–time slaps. This allows the possibility to do a local mesh refinement in the space–time domain, see for example [23].

In this paper we consider a decomposition of the space–time cylinder into finite elements. In particular for spatial domains $\Omega \subset \mathbb{R}^3$ the space–time cylinder is a four–dimensional object, which has to be decomposed into finite elements. In [5], an algorithm based on a Delaunay triangulation is given to construct a four–dimensional pentatope based space–time slap. Here, we present an algorithm to consider arbitrary finite element discretizations of the space–time cylinder, i.e., our approach does not rely on the use of time slaps. This results in a rather flexible approach including adaptive meshes which can move in time. For this we discuss the decomposition of a pentatope into smaller ones. In fact, our approach generalizes the Freudenthal algorithm in $\mathbb{R}^4$ [6, 11, 12]. As initial decomposition we may consider either a decomposition of a hypercube into pentatopes [4, 13, 17], or an extension of a spatial finite element mesh in the space–time cylinder, see, e.g., [5].
For the approximation of the transient partial differential equation in the space–time cylinder we consider a discontinuous Galerkin finite element method. In particular, we apply an interior penalty approach in space [2, 3, 18], and an upwind technique in time [24].
This paper is organised as follows. In the second chapter we describe the discontinuous Galerkin finite element method to solve the transient heat equation as a model problem, and we present a related stability and error analysis. The core part of this paper and the main results are given in the third chapter where we describe an algorithm to decompose a pentatope into smaller ones. As initial decomposition we consider a decomposition of a four–dimensional hypercube into pentatopes. Some numerical results are given in the fourth chapter which underline the applicability of the proposed approach. We close the paper with some conclusions and comments on further work.

2 Discontinuous Galerkin methods

Let $\Omega \subset \mathbb{R}^n$, $n = 1, 2, 3$, be a bounded domain with boundary $\Gamma := \partial\Omega$. As a model problem we consider the transient heat equation

$$\begin{aligned} \partial_t u(\boldsymbol{x}, t) - \Delta u(\boldsymbol{x}, t) &= f(\boldsymbol{x}, t) \quad \text{for } (\boldsymbol{x}, t) \in Q := \Omega \times (0, T), && (2.1)\\ u(\boldsymbol{x}, t) &= 0 \quad \text{for } (\boldsymbol{x}, t) \in \Sigma := \Gamma \times (0, T), && (2.2)\\ u(\boldsymbol{x}, 0) &= u_0(\boldsymbol{x}) \quad \text{for } (\boldsymbol{x}, t) \in \Sigma_0 := \Omega \times \{0\}. && (2.3) \end{aligned}$$

To derive a discrete variational formulation we need to decompose the space–time cylinder $Q = \Omega \times (0, T) \subset \mathbb{R}^{n+1}$ into simplices of mesh size h. For this we assume that the space–time cylinder Q has a polygonal ($n = 1$), a polyhedral ($n = 2$), or a polychoral ($n = 3$) boundary ∂Q. Let $\{\mathcal{T}_N\}_{N\in\mathbb{N}}$ be a sequence of decompositions

$$\overline{Q} = \overline{\mathcal{T}}_N = \bigcup_{k=1}^{N} \overline{\tau}_k$$

into finite elements τ_k of mesh size h_k. We use the simplest possible finite elements, which are triangles for $n = 1$, tetrahedrons for $n = 2$, or pentatopes for the case $n = 3$.

Definition 2.1 (Admissible decomposition) *A decomposition $\mathcal{T}_N$ is called admissible, if two neighbouring elements join either an edge ($n = 1, 2, 3$), a triangle ($n = 2, 3$), or a tetrahedron ($n = 3$). We say that two elements are neighbouring elements, if the intersection of the closure of the two elements is a m–dimensional manifold with $m \leq n$.*

Definition 2.2 (Interior element) *Let $\mathcal{T}_N$ be a decomposition of the space–time cylinder Q into finite elements τ_k. For two neighbouring elements $\tau_k, \tau_\ell \in \mathcal{T}_N$ we define*

$$\Gamma_{k\ell} := \overline{\tau}_k \cap \overline{\tau}_\ell$$

to be an interior element, if $\Gamma_{k\ell}$ is a n–dimensional manifold. The set of all interior elements of the decomposition $\mathcal{T}_N$ will be denoted by $\mathcal{I}_N$.

Any interior element $\Gamma_{k\ell}$ has an exterior normal vector $\boldsymbol{n}_{k\ell}$ with a non–unique direction. We fix the direction of the normal vector such that $\boldsymbol{n}_{k\ell}$ is the exterior normal vector of the element τ_k when $k < \ell$, see Fig. 1. So the direction of the normal vector $\boldsymbol{n}_{k\ell}$ depends on the ordering of the finite elements, but the variational formulation which we are going to use will be independent of this ordering.

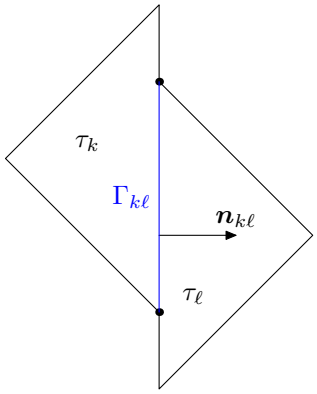

Figure 1: Interior element $\Gamma_{k\ell}$ with normal vector $\boldsymbol{n}_{k\ell}$ for $n = 1$.

Definition 2.3 (Jump, mean value) *For a given function v, the jump across an interior element $\Gamma_{k\ell}$, $k < \ell$, is defined as*

$$[v]_{\Gamma_{k\ell}}(\boldsymbol{x}, t) := v_{|\tau_k}(\boldsymbol{x}, t) - v_{|\tau_\ell}(\boldsymbol{x}, t) \qquad \text{for all } (\boldsymbol{x}, t) \in \Gamma_{k\ell},$$

and the average of v is given by

$$\langle v \rangle_{\Gamma_{k\ell}}(\boldsymbol{x}, t) := \frac{1}{2}\left[v_{|\tau_k}(\boldsymbol{x}, t) + v_{|\tau_\ell}(\boldsymbol{x}, t)\right] \quad \text{for all } (\boldsymbol{x}, t) \in \Gamma_{k\ell}.$$

Definition 2.4 (Upwind) *Let $\Gamma_{k\ell}$ be an interior element of the decomposition $\mathcal{T}_N$ with the normal vector $\boldsymbol{n}_{k\ell} = (n_x, n_t)^\top$. The upwind of a given function v is then given by*

$$v^{\rm up}(\boldsymbol{x},t) := \begin{cases} v_{|\tau_k}(\boldsymbol{x},t) & \text{for } n_t \geq 0, \\ v_{|\tau_\ell}(\boldsymbol{x},t) & \text{for } n_t < 0 \end{cases} \quad \text{for all } (\boldsymbol{x},t) \in \Gamma_{k\ell}.$$

Although the jump and the upwind of a function v depend on the ordering of the finite elements τ_k and τ_ℓ, the variational formulation of the initial boundary value problem (2.1)–(2.3) will be independent of the choice of the particular ordering.
For a finite element $\tau_k \in \mathcal{T}_N$ and for $s_{\boldsymbol{x}}, s_t \in \mathbb{N}_0$ we introduce the anisotropic Sobolev space

$$H^{s_{\boldsymbol{x}},s_t}(\tau_k) := \big\{ v \in L_2(\tau_k) : D^{\boldsymbol{\alpha}_{\boldsymbol{x}}} D^{\alpha_t} v \in L_2(\tau_k) \text{ for all } |\boldsymbol{\alpha}_{\boldsymbol{x}}| \leq s_{\boldsymbol{x}}, \alpha_t \leq s_t, \\ |\boldsymbol{\alpha}_{\boldsymbol{x}}| + \alpha_t \leq \max\{s_{\boldsymbol{x}}, s_t\} \big\}$$

where $\boldsymbol{\alpha}_{\boldsymbol{x}} \in \mathbb{N}_0^n$ is a multi–index, and $\alpha_t \in \mathbb{N}_0$. The related norm and semi–norm are given by

$$\|v\|_{H^{s_{\boldsymbol{x}},s_t}(\tau_k)} := \left[\sum_{\substack{|\boldsymbol{\alpha}_{\boldsymbol{x}}| \leq s_{\boldsymbol{x}}, \alpha_t \leq s_t \\ |\boldsymbol{\alpha}_{\boldsymbol{x}}| + \alpha_t \leq \max\{s_{\boldsymbol{x}}, s_t\}}} \|D_{\boldsymbol{x}}^{\boldsymbol{\alpha}_{\boldsymbol{x}}} D_t^{\alpha_t} v\|_{L_2(\tau_k)}^2 \right]^{1/2},$$

$$|v|_{H^{s_{\boldsymbol{x}},s_t}(\tau_k)} := \left[\sum_{\substack{|\boldsymbol{\alpha}_{\boldsymbol{x}}| \leq s_{\boldsymbol{x}}, \alpha_t \leq s_t \\ |\boldsymbol{\alpha}_{\boldsymbol{x}}| + \alpha_t = \max\{s_{\boldsymbol{x}}, s_t\}}} \|D_{\boldsymbol{x}}^{\boldsymbol{\alpha}_{\boldsymbol{x}}} D_t^{\alpha_t} v\|_{L_2(\tau_k)}^2 \right]^{1/2}.$$

Remark 2.1 *In the particular case $s_{\boldsymbol{x}} = s_t = s \in \mathbb{N}_0$, the anisotropic Sobolev space $H^{s_{\boldsymbol{x}},s_t}(\tau_k)$ coincides with the usual Sobolev space $H^s(\tau_k)$.*

Definition 2.5 (Broken Sobolev space) *Let $\mathcal{T}_N$ be a decomposition of Q into finite elements τ_k, $k = 1, \ldots, N$. For $s_{\boldsymbol{x}}, s_t \in \mathbb{N}_0$ the broken Sobolev space is given by*

$$H^{s_{\boldsymbol{x}},s_t}(\mathcal{T}_N) := \big\{ v \in L_2(Q) : v_{|\tau_k} \in H^{s_{\boldsymbol{x}},s_t}(\tau_k) \text{ for all } \tau_k \in \mathcal{T}_N \big\},$$

where

$$\|v\|_{H^{s_{\boldsymbol{x}},s_t}(\mathcal{T}_N)} := \left[\sum_{k=1}^N \|v\|_{H^{s_{\boldsymbol{x}},s_t}(\tau_k)}^2 \right]^{1/2}, \quad |v|_{H^{s_{\boldsymbol{x}},s_t}(\mathcal{T}_N)} := \left[\sum_{k=1}^N |v|_{H^{s_{\boldsymbol{x}},s_t}(\tau_k)}^2 \right]^{1/2}$$

are the related norm and semi–norm, respectively.

For a decomposition $\mathcal{T}_N$ of the space–time cylinder Q we introduce the discrete function space

$$S_{h,0}^p(\mathcal{T}_N) := \big\{ v : v_{|\tau_k} \in \mathbb{P}_p(\tau_k) \text{ for all } \tau_k \in \mathcal{T}_N \text{ and } v_{|\Sigma} = 0 \big\}$$

of local polynomials of degree p. To derive a discrete variational formulation for the initial boundary value problem (2.1)–(2.3) we use an interior penalty Galerkin approach for the Laplacian, and an upwind technique for the time derivative, see, e.g., [16, 18]. Hence we have to find $u_h \in S^p_{h,0}(\mathcal{T}_N)$ such that

$$
\begin{aligned}
a_{DG}(u_h, v_h) &:= -\sum_{k=1}^{N} \int_{\tau_k} u_h(\boldsymbol{x},t)\partial_t v_h(\boldsymbol{x},t) d\boldsymbol{x}dt + \int_{\Sigma_T} u_h(\boldsymbol{x},t) v_h(\boldsymbol{x},t) ds_{(\boldsymbol{x},t)} \\
&+ \sum_{\Gamma_{k\ell}\in\mathcal{I}_N} \int_{\Gamma_{k\ell}} n_t\, u_h^{\mathrm{up}}(\boldsymbol{x},t)\, [v_h]_{\Gamma_{k\ell}}(\boldsymbol{x},t) ds_{(\boldsymbol{x},t)} + \sum_{k=1}^{N} \int_{\tau_k} \nabla_{\boldsymbol{x}} u_h(\boldsymbol{x},t)\cdot\nabla_{\boldsymbol{x}} v_h(\boldsymbol{x},t) d\boldsymbol{x}dt \\
&+ \sum_{\Gamma_{k\ell}\in\mathcal{I}_N} \frac{\sigma}{|\Gamma_{k\ell}|^{\beta}} \int_{\Gamma_{k\ell}} |\boldsymbol{n}_{\boldsymbol{x}}|^2 [u_h]_{\Gamma_{k\ell}}(\boldsymbol{x},t)\, [v_h]_{\Gamma_{k\ell}}(\boldsymbol{x},t) ds_{(\boldsymbol{x},t)} \\
&- \sum_{\Gamma_{k\ell}\in\mathcal{I}_N} \int_{\Gamma_{k\ell}} \big[\langle \boldsymbol{n}_{\boldsymbol{x}}\cdot\nabla_{\boldsymbol{x}} u_h\rangle_{\Gamma_{k\ell}}(\boldsymbol{x},t)\, [v_h]_{\Gamma_{k\ell}}(\boldsymbol{x},t) - \varepsilon\, [u_h]_{\Gamma_{k\ell}}(\boldsymbol{x},t)\, \langle \boldsymbol{n}_{\boldsymbol{x}}\cdot\nabla_{\boldsymbol{x}} v_h\rangle_{\Gamma_{k\ell}}(\boldsymbol{x},t)\big] ds_{(\boldsymbol{x},t)} \\
&= \int_Q f(\boldsymbol{x},t) v_h(\boldsymbol{x},t) d\boldsymbol{x}dt + \int_{\Sigma_0} u_0(\boldsymbol{x},t) v_h(\boldsymbol{x},t) ds_{(\boldsymbol{x},t)}
\end{aligned}
\tag{2.4}
$$

is satisfied for all $v_h \in S^p_{h,0}(\mathcal{T}_N)$. Note that σ, β, and ε are parameters to be chosen appropriately. For $v \in H^{s_{\boldsymbol{x}},s_t}(\mathcal{T}_N)$ with $s_{\boldsymbol{x}}, s_t \geq 1$ and $\sigma > 0$, the related energy norm is given by

$$
\|v\|^2_{DG} := \|v\|^2_A + \|v\|^2_B,
$$

where

$$
\begin{aligned}
\|v\|^2_A &:= |v|^2_{H^{1,0}(\mathcal{T}_N)} + \sum_{\Gamma_{k\ell}\in\mathcal{I}_N} \frac{\sigma}{|\Gamma_{k\ell}|^{\beta}} \big\| |\boldsymbol{n}_{\boldsymbol{x}}|\, [v]_{\Gamma_{k\ell}} \big\|^2_{L_2(\Gamma_{k\ell})}, \\
\|v\|^2_B &:= \sum_{k=1}^{N} h_k \|v\|^2_{H^{0,1}(\tau_k)} + \frac{1}{2}\left[\|v\|^2_{L_2(\Sigma_0\cup\Sigma_T)} + \sum_{\Gamma_{k\ell}\in\mathcal{I}_N} \Big\| \sqrt{|n_t|}\, [u]_{\Gamma_{k\ell}} \Big\|^2_{L_2(\Gamma_{k\ell})} \right].
\end{aligned}
$$

Now we are in a position to establish unique solvability of the variational formulation (2.4) which is based on the following stability result.

Theorem 2.6 *Let $\varepsilon \in \{-1, 0, 1\}$, $\beta = 1/n$, and $\sigma > 0$. For $\varepsilon \in \{-1, 0\}$ let σ be sufficient large. Then the stability estimate*

$$
\sup_{0\neq v_h \in S^p_{h,0}(\mathcal{T}_N)} \frac{a_{DG}(u_h, v_h)}{\|v_h\|_{DG}} \geq c_1^A \|u_h\|_{DG} \quad \textit{for all } u_h \in S^p_{h,0}(\mathcal{T}_N)
$$

is satisfied.

Proof. The proof follows as in [18], by using the technique as in [10]; see also [16]. ∎

Based on the stability result as given in Theorem 2.6 we can ensure unique solvability of the variational formulation (2.4), and we can derive a priori error estimates. In particular, let $u \in H^{\min\{s_{\boldsymbol{x}},s_t\}}(\mathcal{T}_N) = H^{\min\{s_{\boldsymbol{x}},s_t\},\min\{s_{\boldsymbol{x}},s_t\}}(\mathcal{T}_N)$ be the exact solution of the initial boundary value problem (2.1)–(2.3). We then conclude the energy error estimate

$$\|u - u_h\|_{DG} \leq ch^{\min\{s_{\boldsymbol{x}},s_t,p+1\}-1} \, |u|_{H^{\min\{s_{\boldsymbol{x}},s_t\}}(\mathcal{T}_N)} \, ,$$

and by applying the Aubin–Nitsche trick, for $\varepsilon = -1$,

$$\|u - u_h\|_{L_2(Q)} \leq ch^{\min\{s_{\boldsymbol{x}},s_t,p+1\}} \, |u|_{H^{\min\{s_{\boldsymbol{x}},s_t\}}(\mathcal{T}_N)} \, . \tag{2.5}$$

3 Pentatope space–time decompositions

To apply the discontinuous Galerkin finite element method as described before in particular for three–dimensional spatial domains $\Omega \subset \mathbb{R}^3$ we need to have a decomposition of the space–time cylinder $Q = \Omega \times (0,T)$ in the four–dimensional space. To be most flexible, and to allow local refinements, we now describe a technique to decompose a given pentatope into smaller ones. For this we first describe the refinement of a tetrahedron in $\mathbb{R}^4$.

3.1 Decomposing a tetrahedron

We first recall the definition of a tetrahedron in $\mathbb{R}^4$.

Definition 3.1 (Tetrahedron) *Let $\boldsymbol{x}_i \in \mathbb{R}^4$, $i = 1, \ldots, 4$, be given nodes, such that the vectors*

$$\boldsymbol{x}_2 - \boldsymbol{x}_1, \quad \boldsymbol{x}_3 - \boldsymbol{x}_1, \quad \boldsymbol{x}_4 - \boldsymbol{x}_1$$

are linear independent. Then the convex hull

$$\sigma := \operatorname{conv}(\boldsymbol{x}_1, \boldsymbol{x}_2, \boldsymbol{x}_3, \boldsymbol{x}_4)$$

defines a tetrahedron in $\mathbb{R}^4$.

If we introduce the reference tetrahedron

$$\begin{aligned} \hat{\sigma} := \big\{ \boldsymbol{\xi} = (\xi_1, \xi_2, \xi_3)^\top \in \mathbb{R}^3 : \quad & 0 \leq \xi_1 \leq 1, \\ & 0 \leq \xi_2 \leq 1 - \xi_1, \\ & 0 \leq \xi_3 \leq 1 - \xi_1 - \xi_2 \big\}, \end{aligned}$$

we can write $\boldsymbol{x} \in \sigma$ as

$$\boldsymbol{x} = \boldsymbol{x}_1 + J_T \boldsymbol{\xi} \quad \text{for } \boldsymbol{\xi} \in \hat{\sigma},$$

where

$$J_T := \begin{pmatrix} \boldsymbol{x}_{2,1} - \boldsymbol{x}_{1,1} & \boldsymbol{x}_{3,1} - \boldsymbol{x}_{1,1} & \boldsymbol{x}_{4,1} - \boldsymbol{x}_{1,1} \\ \boldsymbol{x}_{2,2} - \boldsymbol{x}_{1,2} & \boldsymbol{x}_{3,2} - \boldsymbol{x}_{1,2} & \boldsymbol{x}_{4,2} - \boldsymbol{x}_{1,2} \\ \boldsymbol{x}_{2,3} - \boldsymbol{x}_{1,3} & \boldsymbol{x}_{3,3} - \boldsymbol{x}_{1,3} & \boldsymbol{x}_{4,3} - \boldsymbol{x}_{1,3} \\ \boldsymbol{x}_{2,4} - \boldsymbol{x}_{1,4} & \boldsymbol{x}_{3,4} - \boldsymbol{x}_{1,4} & \boldsymbol{x}_{4,4} - \boldsymbol{x}_{1,4} \end{pmatrix}.$$

The tranformation matrix $J_T \in \mathbb{R}^{4\times 3}$ is obviously not invertible. However, by Definition 3.1 we have rang$J_T = 3$, and therefore we can compute the pseudoinverse

$$J_T^+ = (J_T^\top J_T)^{-1} J_T^\top,$$

and we obtain a mapping from the tetrahedron σ to the reference tetrahedron $\hat{\sigma}$ by

$$\boldsymbol{\xi} = J_T^+(\boldsymbol{x}_1 - \boldsymbol{x}) \in \hat{\sigma} \quad \text{for } \boldsymbol{x} \in \sigma.$$

Within the variational formulation (2.4) we need to have the exterior normal vector $\boldsymbol{n}$ of a tetrahedron, which can be obtained by using the generalized cross product.

Definition 3.2 (Normal vector) *Let σ be a tetrahedron with nodes $\boldsymbol{x}_i \in \mathbb{R}^4$, $i = 1, \ldots, 4$. The normal vector $\boldsymbol{n}$ of the tetrahedron σ is given by*

$$\boldsymbol{n} := \begin{vmatrix} \boldsymbol{e}_1 & \boldsymbol{e}_2 & \boldsymbol{e}_3 & \boldsymbol{e}_4 \\ \boldsymbol{x}_{2,1} - \boldsymbol{x}_{1,1} & \boldsymbol{x}_{2,2} - \boldsymbol{x}_{1,2} & \boldsymbol{x}_{2,3} - \boldsymbol{x}_{1,3} & \boldsymbol{x}_{2,4} - \boldsymbol{x}_{1,4} \\ \boldsymbol{x}_{3,1} - \boldsymbol{x}_{1,1} & \boldsymbol{x}_{3,2} - \boldsymbol{x}_{1,2} & \boldsymbol{x}_{3,3} - \boldsymbol{x}_{1,3} & \boldsymbol{x}_{3,4} - \boldsymbol{x}_{1,4} \\ \boldsymbol{x}_{4,1} - \boldsymbol{x}_{1,1} & \boldsymbol{x}_{4,2} - \boldsymbol{x}_{1,2} & \boldsymbol{x}_{4,3} - \boldsymbol{x}_{1,3} & \boldsymbol{x}_{4,4} - \boldsymbol{x}_{1,4} \end{vmatrix},$$

where $\boldsymbol{e}_i$ are the unit vectors of the canonical basis. Note that for the computation of the determinant the vectors $\boldsymbol{e}_i$ are formally seen as scalars.

Next we recall the decomposition of a tetrahedron into eight smaller ones. Although this is rather standard in three–dimensional finite element computations, we give the basic concept which is later transferred to the decomposition of pentatops. First we numerize the nodes of the tetrahedron from 1 to 4, and the midpoints of the six edges from 5 to 10, see Fig. 2. In every corner of the tetrahedron we get one smaller tetrahedron, if we use the corner point and the three midpoints of the adjecent edges, see Fig. 3.

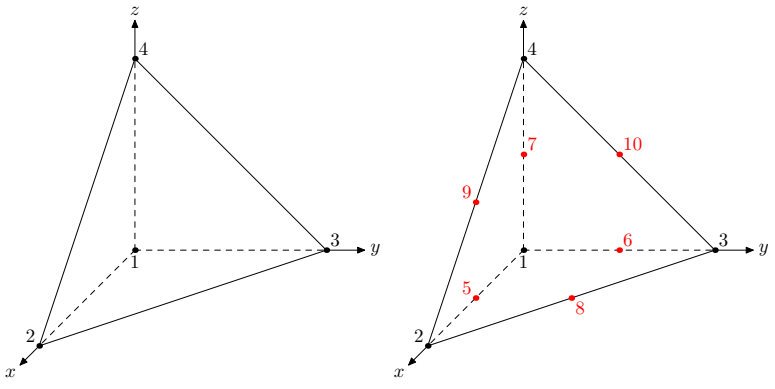

Figure 2: Tetrahedron with corner nodes and midpoints.

Hence we end up with an irregular octahedron as shown in Fig. 3. This octahedron can be decomposed into four smaller tetrahedrons if it is splitted first into two pyramids,

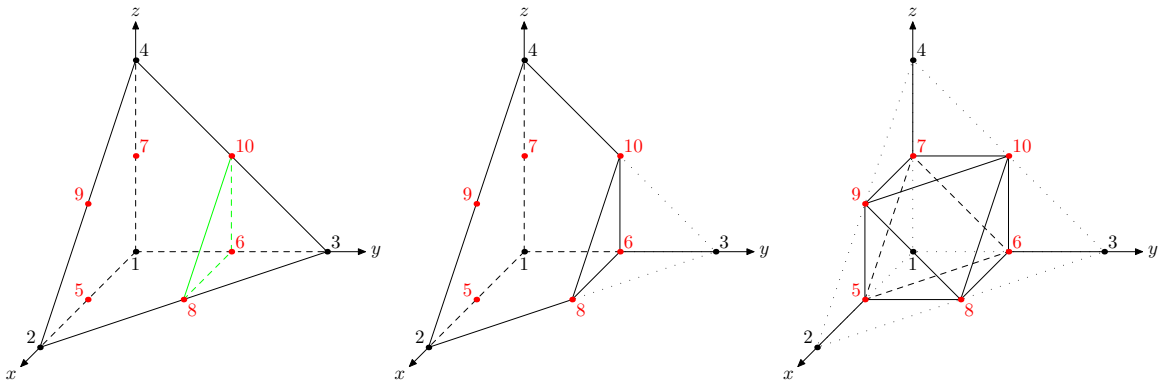

Figure 3: Removing smaller tetrahedrons in corner points.

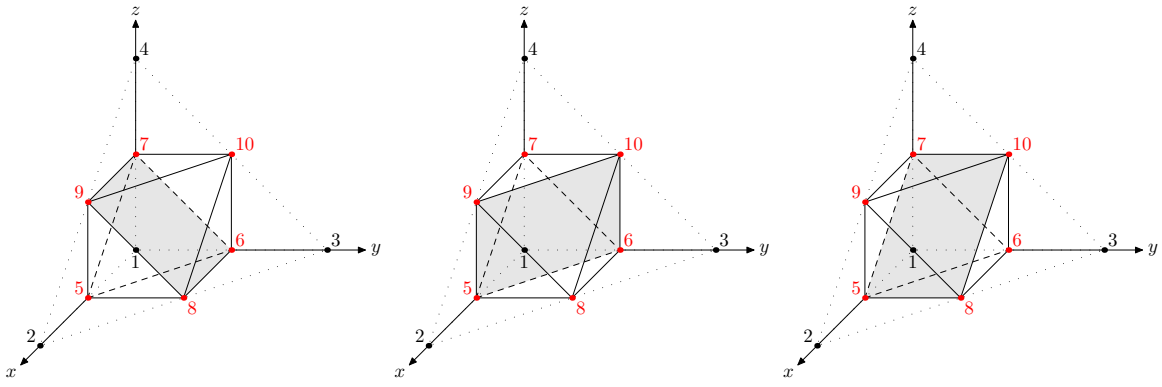

Figure 4: Splitting an octahedron into two pyramids.

and then splitting each pyramid into two tetrahedrons. But there are three different possibilities to split an octahedron into two pyramids, see Fig. 4, which result in three different decompositions of a given tetrahedron into smaller ones.
Each decomposition corresponds to one of the three edges

$$(\boldsymbol{x}_5, \boldsymbol{x}_{10}), \quad (\boldsymbol{x}_6, \boldsymbol{x}_9), \quad (\boldsymbol{x}_7, \boldsymbol{x}_8).$$

If we fix one of these edges, then also the decomposition of the tetrahedron is fixed. This motivates the following definition.

Definition 3.3 (Interior edges) *Let σ be a tetrahedron with nodes $\boldsymbol{x}_i \in \mathbb{R}^4$, $i = 1, \dots, 4$. Further let $\boldsymbol{x}_m \in \mathbb{R}^4$, $m = 5, \dots, 10$, be the midpoints of the six edges of the tetrahedron, which are numerized such that for $1 \leq i < j \leq 4$ the node $\boldsymbol{x}_m$ is the midpoint of the edge $(\boldsymbol{x}_i, \boldsymbol{x}_j)$ with*

$$m = (i-1)\left(3 - \frac{i}{2}\right) + j + 3.$$

Then the edges

$$\Phi := \{(\boldsymbol{x}_5, \boldsymbol{x}_{10}), (\boldsymbol{x}_6, \boldsymbol{x}_9), (\boldsymbol{x}_7, \boldsymbol{x}_8)\}$$

are called the interior edges of the tetrahedron σ.

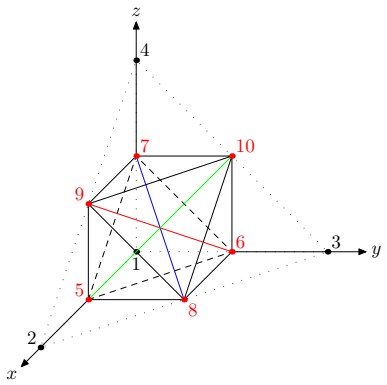

Figure 5: Interior edges Φ of the tetrahedron σ.

Recall that the interior edges as shown in Fig. 5 are the largest edges of the decomposition. In general, the interior edges have not the same length. Hence, to guarantee a shape regular decomposition of the tetrahedron, we have to choose the smallest interior edge $e \in \Phi$, i.e.

$$e = \arg\min_{e_n \in \Phi} |e_n|,$$

to fix the decomposition of the tetrahedron.

3.2 Decomposing a pentatope

In this section we present an approach to decompose a pentatope into 16 smaller pentatopes. For this we first consider a decomposition of the boundary of the pentatope, which consists of five tetrahedra. Since the decomposition of a tetrahedron is not unique, there are several possibilities to decompose the boundary of a pentatope. If the boundary is refined in a suitable way, we are able to refine the pentatope into 16 smaller pentatopes. In [11], Freudenthal presented an algorithm to decompose a n–dimensional simplex into 2^n smaller simplices. For a pentatope the algorithm of Freudenthal gives twelve different possible decompositions of a pentatope. With the present approach we obtain more possible decompositions of a pentatope into $2^4 = 16$ smaller pentatopes. But first we give the definition of a pentatope.

Definition 3.4 (Pentatope) *Let $\boldsymbol{x}_i \in \mathbb{R}^4$, $i = 1, \ldots, 5$, be given nodes, such that the vectors*

$$\boldsymbol{x}_2 - \boldsymbol{x}_1, \quad \boldsymbol{x}_3 - \boldsymbol{x}_1, \quad \boldsymbol{x}_4 - \boldsymbol{x}_1, \quad \boldsymbol{x}_5 - \boldsymbol{x}_1$$

are linear independent. Then the convex hull

$$\tau := \operatorname{conv}(\boldsymbol{x}_1, \ldots, \boldsymbol{x}_5)$$

defines a pentatope.

Other names for pentatopes are 5–cell, pentachoron, hyperpyramid or 4–simplex. In Fig. 6 we give two possible projections of a pentatope. The number n_B of boundary tetrahedrons, the number n_T of triangles, and the number n_E of edges of a pentatope are given by

$$n_B = \binom{5}{4} = \binom{5}{1} = 5, \quad n_T = \binom{5}{3} = \binom{5}{2} = 10, \quad n_E = \binom{5}{2} = 10.$$

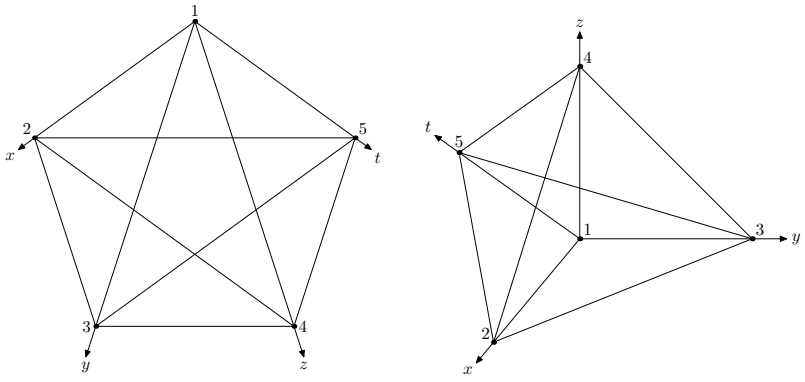

Figure 6: Two possible projections of a pentatope.

If we introduce the reference penatope

$$\hat{\tau} := \big\{\boldsymbol{\xi} = (\xi_1, \xi_2, \xi_3, \xi_4)^\top \in \mathbb{R}^4 : \quad 0 \le \xi_1 \le 1, \\ 0 \le \xi_2 \le 1 - \xi_1, \\ 0 \le \xi_3 \le 1 - \xi_1 - \xi_2, \\ 0 \le \xi_4 \le 1 - \xi_1 - \xi_2 - \xi_3\big\},$$

we can write $\boldsymbol{x} \in \tau$ as

$$\boldsymbol{x} = \boldsymbol{x}_1 + J_P \boldsymbol{\xi} \quad \text{for } \boldsymbol{\xi} \in \hat{\tau}, \tag{3.1}$$

where

$$J_P := \begin{pmatrix} \boldsymbol{x}_{2,1} - \boldsymbol{x}_{1,1} & \boldsymbol{x}_{3,1} - \boldsymbol{x}_{1,1} & \boldsymbol{x}_{4,1} - \boldsymbol{x}_{1,1} & \boldsymbol{x}_{5,1} - \boldsymbol{x}_{1,1} \\ \boldsymbol{x}_{2,2} - \boldsymbol{x}_{1,2} & \boldsymbol{x}_{3,2} - \boldsymbol{x}_{1,2} & \boldsymbol{x}_{4,2} - \boldsymbol{x}_{1,2} & \boldsymbol{x}_{5,2} - \boldsymbol{x}_{1,2} \\ \boldsymbol{x}_{2,3} - \boldsymbol{x}_{1,3} & \boldsymbol{x}_{3,3} - \boldsymbol{x}_{1,3} & \boldsymbol{x}_{4,3} - \boldsymbol{x}_{1,3} & \boldsymbol{x}_{5,3} - \boldsymbol{x}_{1,3} \\ \boldsymbol{x}_{2,4} - \boldsymbol{x}_{1,4} & \boldsymbol{x}_{3,4} - \boldsymbol{x}_{1,4} & \boldsymbol{x}_{4,4} - \boldsymbol{x}_{1,4} & \boldsymbol{x}_{5,4} - \boldsymbol{x}_{1,4} \end{pmatrix}$$

is the Jacobian which is invertible. The volume Δ_τ of a pentatope τ is then given by

$$\Delta_\tau = \int_\tau d\boldsymbol{x} = \int_{\hat{\tau}} |\det J_P| \, d\boldsymbol{\xi} = \\ = |\det J_P| \int_0^1 \int_0^{1-\xi_1} \int_0^{1-\xi_1-\xi_2} \int_0^{1-\xi_1-\xi_2-\xi_3} d\xi_4 d\xi_3 d\xi_2 d\xi_1 = \frac{1}{24} |\det J_P| \, .$$

We now consider the decomposition of a given pentatope τ. First we numerize the nodes of the pentatope from 1 to 5, and the midpoints of the ten edges from 6 to 15, see Fig. 7.

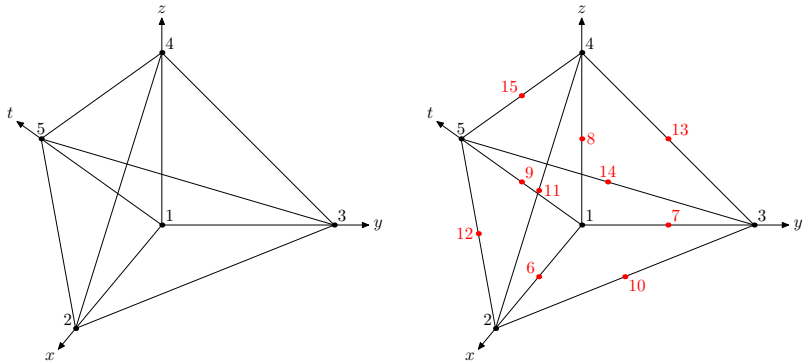

Figure 7: Pentatope with corner nodes and midpoints.

As for the tetrahedron, we first remove the smaller pentatopes in the corner points. For example, in case of the node 3, the related smaller pentatope is given by the node numbers $\{7, 10, 3, 13, 14\}$, which is then removed, see Fig. 8.
If we remove all the smaller pentatopes in the five corner points we end up with the four–dimensional object as shown in Fig. 9 which has to be decomposed into $16 - 5 = 11$ smaller pentatopes.

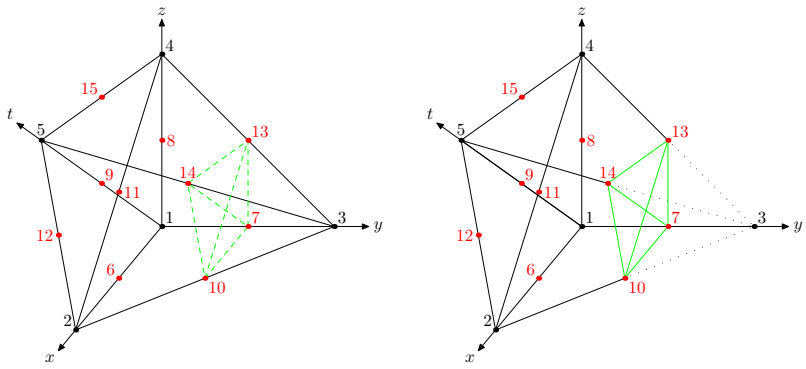

Figure 8: Removing a smaller pentatope in a corner point.

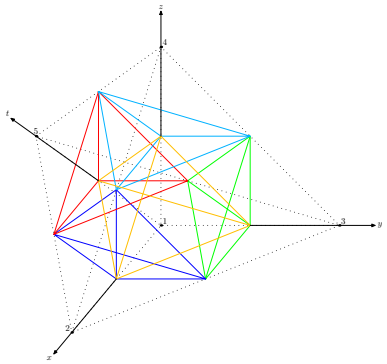

Figure 9: Removing all smaller pentatopes in the corner points.

For this we use the information on the boundary decomposition of the pentatope τ. The five boundary tetrahedrons σ_i, $i = 1, \ldots, 5$, are given by

$$\begin{aligned}
\sigma_1 &:= \operatorname{conv}(\boldsymbol{x}_2, \boldsymbol{x}_3, \boldsymbol{x}_4, \boldsymbol{x}_5), \\
\sigma_2 &:= \operatorname{conv}(\boldsymbol{x}_1, \boldsymbol{x}_3, \boldsymbol{x}_4, \boldsymbol{x}_5), \\
\sigma_3 &:= \operatorname{conv}(\boldsymbol{x}_1, \boldsymbol{x}_2, \boldsymbol{x}_4, \boldsymbol{x}_5), \\
\sigma_4 &:= \operatorname{conv}(\boldsymbol{x}_1, \boldsymbol{x}_2, \boldsymbol{x}_3, \boldsymbol{x}_5), \\
\sigma_5 &:= \operatorname{conv}(\boldsymbol{x}_1, \boldsymbol{x}_2, \boldsymbol{x}_3, \boldsymbol{x}_4).
\end{aligned}$$

Recall that the decomposition of a boundary tetrahedron σ_i depends on the chosen interior edges $e_i \in \Phi_i$, $i = 1, \ldots, 5$, where the possible interior edges for the five boundary tetrahedra are given by

$$\begin{aligned}
\Phi_1 &= \{(\boldsymbol{x}_{10}, \boldsymbol{x}_{15}), (\boldsymbol{x}_{11}, \boldsymbol{x}_{14}), (\boldsymbol{x}_{12}, \boldsymbol{x}_{13})\}, \\
\Phi_2 &= \{(\boldsymbol{x}_7, \boldsymbol{x}_{15}), (\boldsymbol{x}_8, \boldsymbol{x}_{14}), (\boldsymbol{x}_9, \boldsymbol{x}_{13})\}, \\
\Phi_3 &= \{(\boldsymbol{x}_6, \boldsymbol{x}_{15}), (\boldsymbol{x}_8, \boldsymbol{x}_{12}), (\boldsymbol{x}_9, \boldsymbol{x}_{11})\}, \\
\Phi_4 &= \{(\boldsymbol{x}_6, \boldsymbol{x}_{14}), (\boldsymbol{x}_7, \boldsymbol{x}_{12}), (\boldsymbol{x}_9, \boldsymbol{x}_{10})\}, \\
\Phi_5 &= \{(\boldsymbol{x}_6, \boldsymbol{x}_{13}), (\boldsymbol{x}_7, \boldsymbol{x}_{11}), (\boldsymbol{x}_8, \boldsymbol{x}_{10})\}.
\end{aligned}$$

So we have to choose for each boundary tetrahedron σ_i an interior edge $e_i \in \Phi_i$. This motivates the following definitions.

Definition 3.5 (Fixed edges) *Let τ be a pentatope with nodes $\boldsymbol{x}_i \in \mathbb{R}^4$, $i = 1, \ldots, 5$. The interior edges $e_i \in \Phi_i$ belonging to the set*

$$\phi := \left\{ e_{i_1}, \ldots, e_{i_5} : e_{i_j} \in \Phi_i, i = 1, \ldots, 5 \right\}$$

are called fixed edges of ϕ. In fact, ϕ involves one particular edge chosen from each Φ_i.

Definition 3.6 *Let $A = \{e_1, \ldots, e_n\}$ be a set with $n \in \mathbb{N}$ edges $e_i = (x_{i_1}, x_{i_2})$. The mapping* nodes *creates the set of all nodes of the edges $e_i \in A$, i.e.,*

$$\operatorname{nodes}(A) := \bigcup_{e_i = (\boldsymbol{x}_{i_1}, \boldsymbol{x}_{i_2}) \in A} \{\boldsymbol{x}_{i_1}, \boldsymbol{x}_{i_2}\}.$$

Definition 3.7 (Fixed nodes) *Let τ be a pentatope with nodes $\boldsymbol{x}_i \in \mathbb{R}^4$, $i = 1, \ldots, 5$, and let ϕ be a set of fixed edges. Then the nodes of all the fixed edges in ϕ,*

$$x_\phi := \operatorname{nodes}(\phi),$$

are called fixed nodes of τ.

Overall there are $3^5 = 243$ possible sets of fixed edges, where each of the sets corresponds to a possible decomposition of the boundary of a pentatope τ. But not for all possible sets of fixed edges there exists an admissible decomposition of the pentatope into 16 smaller pentatopes. In this paper we present, for a particular class of these 243 possible sets, methods to decompose the pentatope τ, where we use information of the fixed edges.
One possible set of fixed edges for the pentatope as shown in Fig. 7 is

$$\phi_1 := \{(\boldsymbol{x}_{10}, \boldsymbol{x}_{15}), (\boldsymbol{x}_9, \boldsymbol{x}_{13}), (\boldsymbol{x}_6, \boldsymbol{x}_{15}), (\boldsymbol{x}_9, \boldsymbol{x}_{10}), (\boldsymbol{x}_6, \boldsymbol{x}_{13})\}\,.$$

Note that the graph of ϕ_1 is connected and cyclic. As an example for a connected but non–cyclic graph we may consider

$$\phi_2 = \{(\boldsymbol{x}_{10}, \boldsymbol{x}_{15}), (\boldsymbol{x}_9, \boldsymbol{x}_{13}), (\boldsymbol{x}_9, \boldsymbol{x}_{11}), (\boldsymbol{x}_9, \boldsymbol{x}_{10}), (\boldsymbol{x}_8, \boldsymbol{x}_{10})\}\,.$$

In the following we are going to construct decompositions for sets of fixed edges where the edges are connected. This motivates the following definition.

Definition 3.8 (Connected fixing) *Let τ be a pentatope, and let ϕ be a set of related fixed edges. If the set ϕ satisfies the property that*

$$\textit{for all edges} \quad e_i \in \phi \quad \textit{there exist an edge} \quad e_j \in \phi \quad \textit{with} \quad i \neq j \ \textit{and} \ e_i \cap e_j \neq \emptyset,$$

then the set ϕ is called a connected fixing of τ.

Obviously, a connected fixing ϕ implies a set of fixed nodes x_ϕ whose dimension is bounded by

$$5 \leq |x_\phi| \leq 6.$$

Therefore we can split up the connected fixings into two classes.

Definition 3.9 (Cyclic and non–cyclic fixing) *Let τ be a pentatope, and let ϕ be a connected fixing of τ. If the number of fixed nodes x_ϕ is given by $|x_\phi| = 5$, then the fixing ϕ is called cyclic fixing. Otherwise, the fixing ϕ is called non–cyclic fixing.*

Out of the 243 possible sets of fixed edges, there are 12 different cyclic fixings, and 75 non–cyclic fixings, for a listing see the Appendix. For a cyclic fixing ϕ of a pentatope τ we now can construct an admissible decomposition.

Definition 3.10 (Cyclic decomposition) *Let τ be a pentatope with nodes $\boldsymbol{x}_i \in \mathbb{R}^4$, $i = 1, \ldots, 5$, and let $\phi = \{e_1, \ldots, e_5\}$ be a cyclic fixing of τ. We further numerize the midpoints $\boldsymbol{x}_m$ of the edges $(\boldsymbol{x}_i, \boldsymbol{x}_j)$, $1 \leq i < j \leq 5$, such that*

$$m = (i-1)\left(4 - \frac{i}{2}\right) + j + 4.$$

We then define the sets of nodes

$$\begin{aligned}
\chi_1 &:= \{\boldsymbol{x}_1, \boldsymbol{x}_6, \boldsymbol{x}_7, \boldsymbol{x}_8, \boldsymbol{x}_9\}, \\
\chi_2 &:= \{\boldsymbol{x}_6, \boldsymbol{x}_2, \boldsymbol{x}_{10}, \boldsymbol{x}_{11}, \boldsymbol{x}_{12}\}, \\
\chi_3 &:= \{\boldsymbol{x}_7, \boldsymbol{x}_{10}, \boldsymbol{x}_3, \boldsymbol{x}_{13}, \boldsymbol{x}_{14}\}, \\
\chi_4 &:= \{\boldsymbol{x}_8, \boldsymbol{x}_{11}, \boldsymbol{x}_{13}, \boldsymbol{x}_4, \boldsymbol{x}_{15}\}, \\
\chi_5 &:= \{\boldsymbol{x}_9, \boldsymbol{x}_{12}, \boldsymbol{x}_{14}, \boldsymbol{x}_{15}, \boldsymbol{x}_5\}, \\
\chi_6 &:= \operatorname{nodes}(\phi) = x_\phi.
\end{aligned}$$

We also define ten different indices $\ell_{i,j}$ *for* $1 \leq i < j \leq 5$ *by*

$$\ell_{i,j} := (i-1)\left(4 - \frac{i}{2}\right) + j + 5.$$

For an index $\ell_{i,j}$, $1 \leq i < j \leq 5$, *we then define the set of nodes* $\chi_{\ell_{i,j}}$ *as*

$$\chi_{\ell_{i,j}} := \operatorname{nodes}\left(\{\mathrm{e_i}\} \cup \{\mathrm{e_j}\}\right) \cup \left[\operatorname{nodes}(\Phi_i) \cap \operatorname{nodes}(\Phi_j)\right] \tag{3.2}$$

where Φ_k *are the possible interior edges of the boundary tetrahedra* σ_k, $k = 1, \ldots, 5$, *and* $e_\ell \in \phi$ *are the fixed interior edges of the cyclic fixing* ϕ. *Then the set of pentatopes*

$$\mathcal{T}_{\mathrm{cycl}} := \{\tau_i = \operatorname{conv}(\chi_i) : i = 1, \ldots, 16\}$$

is called cyclic decomposition of the pentatope τ.

The first five pentatopes of the cyclic decomposition $\mathcal{T}_{\mathrm{cycl}}$ are the smaller pentatopes which are related to the corner nodes. The nodes of the pentatope $\tau_6 \in \mathcal{T}_{\mathrm{cycl}}$ are the fixed nodes of the cyclic fixing ϕ. Since any fixed edge $e_\ell \in \phi$ is part of four new boundary tetrahedra, see Fig. 5, any fixed edge $e_\ell \in \phi$ has to be part in four of the ten remaining smaller pentatopes as well, as expressed in (3.2). If we use the cyclic fixing

$$\phi_1 = \{(\boldsymbol{x}_{10}, \boldsymbol{x}_{15}), (\boldsymbol{x}_9, \boldsymbol{x}_{13}), (\boldsymbol{x}_6, \boldsymbol{x}_{15}), (\boldsymbol{x}_9, \boldsymbol{x}_{10}), (\boldsymbol{x}_6, \boldsymbol{x}_{13})\}$$

to derive the cyclic decomposition $\mathcal{T}_{\mathrm{cycl}}$, we get the following sets of nodes:

$$\begin{aligned}
\chi_1 &:= \{\boldsymbol{x}_1, \boldsymbol{x}_6, \boldsymbol{x}_7, \boldsymbol{x}_8, \boldsymbol{x}_9\}, & \chi_2 &:= \{\boldsymbol{x}_6, \boldsymbol{x}_2, \boldsymbol{x}_{10}, \boldsymbol{x}_{11}, \boldsymbol{x}_{12}\}, \\
\chi_3 &:= \{\boldsymbol{x}_7, \boldsymbol{x}_{10}, \boldsymbol{x}_3, \boldsymbol{x}_{13}, \boldsymbol{x}_{14}\}, & \chi_4 &:= \{\boldsymbol{x}_8, \boldsymbol{x}_{11}, \boldsymbol{x}_{13}, \boldsymbol{x}_4, \boldsymbol{x}_{15}\}, \\
\chi_5 &:= \{\boldsymbol{x}_9, \boldsymbol{x}_{12}, \boldsymbol{x}_{14}, \boldsymbol{x}_{15}, \boldsymbol{x}_5\}, & \chi_6 &:= \{\boldsymbol{x}_6, \boldsymbol{x}_9, \boldsymbol{x}_{10}, \boldsymbol{x}_{13}, \boldsymbol{x}_{15}\}, \\
\chi_7 &:= \{\boldsymbol{x}_6, \boldsymbol{x}_8, \boldsymbol{x}_9, \boldsymbol{x}_{13}, \boldsymbol{x}_{15}\}, & \chi_8 &:= \{\boldsymbol{x}_7, \boldsymbol{x}_9, \boldsymbol{x}_{10}, \boldsymbol{x}_{13}, \boldsymbol{x}_{14}\}, \\
\chi_9 &:= \{\boldsymbol{x}_6, \boldsymbol{x}_7, \boldsymbol{x}_8, \boldsymbol{x}_9, \boldsymbol{x}_{13}\}, & \chi_{10} &:= \{\boldsymbol{x}_9, \boldsymbol{x}_{10}, \boldsymbol{x}_{13}, \boldsymbol{x}_{14}, \boldsymbol{x}_{15}\}, \\
\chi_{11} &:= \{\boldsymbol{x}_6, \boldsymbol{x}_9, \boldsymbol{x}_{10}, \boldsymbol{x}_{12}, \boldsymbol{x}_{15}\}, & \chi_{12} &:= \{\boldsymbol{x}_6, \boldsymbol{x}_8, \boldsymbol{x}_{11}, \boldsymbol{x}_{13}, \boldsymbol{x}_{15}\}, \\
\chi_{13} &:= \{\boldsymbol{x}_6, \boldsymbol{x}_{10}, \boldsymbol{x}_{11}, \boldsymbol{x}_{12}, \boldsymbol{x}_{15}\}, & \chi_{14} &:= \{\boldsymbol{x}_6, \boldsymbol{x}_7, \boldsymbol{x}_9, \boldsymbol{x}_{10}, \boldsymbol{x}_{13}\}, \\
\chi_{15} &:= \{\boldsymbol{x}_9, \boldsymbol{x}_{10}, \boldsymbol{x}_{12}, \boldsymbol{x}_{14}, \boldsymbol{x}_{15}\}, & \chi_{16} &:= \{\boldsymbol{x}_6, \boldsymbol{x}_{10}, \boldsymbol{x}_{11}, \boldsymbol{x}_{13}, \boldsymbol{x}_{15}\}.
\end{aligned}$$

This decomposition is presented as a connectivity graph in Fig. 10. The 16 circles in the graph represent the 16 smaller pentatopes of the decomposition. An edge in the graph connects two circles and so the edges in the graph correspond to the tetrahedra which connect two neighbouring pentatopes. An arrow between two neighbouring pentatopes indicates which two nodes must be exchanged in order to obtain the respective other neighbouring pentatope. Therefore the node numbers of an interior tetrahedron, which connects two neighbouring pentatopes, can be obtained by removing the corresponding node number of the arrow from one of the pentatopes. If we look closer at the graph, we notice that the pentatope τ_6 is connected with five other pentatopes. Thus the pentatope τ_6 is not part of the boundary of the decomposition. The pentatopes $\tau_1, \ldots, \tau_5$, which are the pentatopes related to the corner nodes, are connected with only one pentatope. Therefore four boundary tetrahedra of the decomposition must be part of one of the boundary pentatopes $\tau_1, \ldots, \tau_5$. The new pentatopes $\tau_7, \ldots, \tau_{16}$ are connected with three other pentatopes and thus the pentatopes $\tau_7, \ldots, \tau_{16}$ must include two boundary tetrahedra of the decomposition.

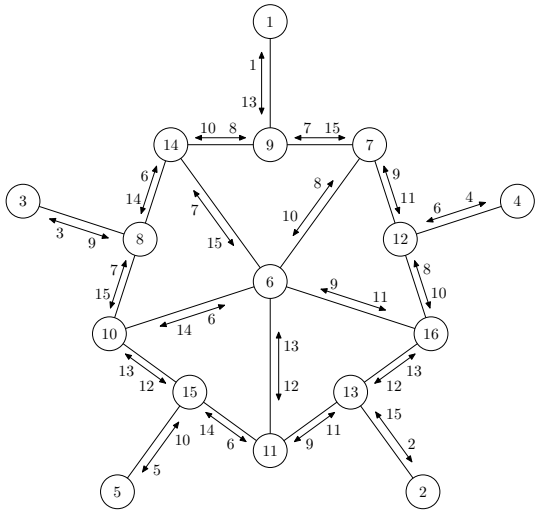

Figure 10: Connectivity graph of a cyclic decomposition of a pentatope.

By using the connectivity graph as shown in Fig. 10 we are able to construct all pentatopes, boundary tetrahedra, and interior tetrahedra of the decomposition. In a similar way it is possible to construct a decomposition of a pentatope τ by using information of a non–cyclic fixing ϕ.

Definition 3.11 (Non–cyclic decomposition) *Let τ be a pentatope with nodes $\boldsymbol{x}_i \in \mathbb{R}^4$, $i = 1, \ldots, 5$, and let $\phi = \{e_1, \ldots, e_5\}$ be a non–cyclic fixing of τ. We further numerize the midpoints $\boldsymbol{x}_m$ of the edges $(\boldsymbol{x}_i, \boldsymbol{x}_j)$, $1 \leq i < j \leq 5$, such that*

$$m = (i-1)\left(4 - \frac{i}{2}\right) + j + 4.$$

In the following we choose two fixed edges e_{i_1}, e_{i_2} from the non–cycling fixing ϕ such that one of the two following properties holds, where

$$M := \{e_i \in \phi : \text{ there exists a node } x \in e_i : x \notin e_j \text{ for all } j \neq i\}.$$

i. If $|M| = 3$, then we choose the two edges $e_{i_1}, e_{i_2} \in M = \{e_{i_1}, e_{i_2}, e_{i_3}\}$ such that

$$\text{nodes}(\Phi_{i_1}) \cap \text{nodes}(\Phi_{i_2}) \cap \text{nodes}(e_{i_3}) \neq \emptyset.$$

ii. If $|M| = 4$, then we choose two different adjacent edges $e_{i_1}, e_{i_2} \in M$, i.e.,

$$e_{i_1} \neq e_{i_2} \quad \text{and} \quad e_{i_1} \cap e_{i_2} \neq \emptyset.$$

We then define the sets of nodes

$$\begin{aligned}
\chi_1 &:= \{\boldsymbol{x}_1, \boldsymbol{x}_6, \boldsymbol{x}_7, \boldsymbol{x}_8, \boldsymbol{x}_9\}, \\
\chi_2 &:= \{\boldsymbol{x}_6, \boldsymbol{x}_2, \boldsymbol{x}_{10}, \boldsymbol{x}_{11}, \boldsymbol{x}_{12}\}, \\
\chi_3 &:= \{\boldsymbol{x}_7, \boldsymbol{x}_{10}, \boldsymbol{x}_3, \boldsymbol{x}_{13}, \boldsymbol{x}_{14}\}, \\
\chi_4 &:= \{\boldsymbol{x}_8, \boldsymbol{x}_{11}, \boldsymbol{x}_{13}, \boldsymbol{x}_4, \boldsymbol{x}_{15}\}, \\
\chi_5 &:= \{\boldsymbol{x}_9, \boldsymbol{x}_{12}, \boldsymbol{x}_{14}, \boldsymbol{x}_{15}, \boldsymbol{x}_5\}.
\end{aligned}$$

Moreover, for any tuple $(i, j) \neq (i_1, i_2)$, $1 \leq i < j \leq 5$, we assign an index $\ell_{i,j} \in \{6, \ldots, 14\}$ and a set

$$\chi_{\ell_{i,j}} := \text{nodes}\left(\{\text{e}_\text{i}\} \cup \{\text{e}_\text{j}\}\right) \cup \left[\text{nodes}(\Phi_i) \cap \text{nodes}(\Phi_j)\right].$$

Further we define

$$\begin{aligned}
\chi_{15} &:= \text{nodes}(\phi \setminus \{e_{i_1}\}), \\
\chi_{16} &:= \text{nodes}(\phi \setminus \{e_{i_2}\}).
\end{aligned}$$

Then the set of pentatopes

$$\mathcal{T}_{\text{ncycl}} := \{\tau_i = \text{conv}(\chi_i) : i = 1, \ldots, 16\}$$

is called non–cyclic decomposition of the pentatope τ.

If we use the non–cyclic fixing

$$\phi_2 = \{(\boldsymbol{x}_{10}, \boldsymbol{x}_{15}), (\boldsymbol{x}_9, \boldsymbol{x}_{13}), (\boldsymbol{x}_9, \boldsymbol{x}_{11}), (\boldsymbol{x}_9, \boldsymbol{x}_{10}), (\boldsymbol{x}_8, \boldsymbol{x}_{10})\}$$

to derive the non–cyclic decomposition $\mathcal{T}_{\text{ncycl}}$ we get the following sets of nodes:

$$\begin{aligned}
\chi_1 &:= \{\boldsymbol{x}_1, \boldsymbol{x}_6, \boldsymbol{x}_7, \boldsymbol{x}_8, \boldsymbol{x}_9\}, & \chi_2 &:= \{\boldsymbol{x}_6, \boldsymbol{x}_2, \boldsymbol{x}_{10}, \boldsymbol{x}_{11}, \boldsymbol{x}_{12}\}, \\
\chi_3 &:= \{\boldsymbol{x}_7, \boldsymbol{x}_{10}, \boldsymbol{x}_3, \boldsymbol{x}_{13}, \boldsymbol{x}_{14}\}, & \chi_4 &:= \{\boldsymbol{x}_8, \boldsymbol{x}_{11}, \boldsymbol{x}_{13}, \boldsymbol{x}_4, \boldsymbol{x}_{15}\}, \\
\chi_5 &:= \{\boldsymbol{x}_9, \boldsymbol{x}_{12}, \boldsymbol{x}_{14}, \boldsymbol{x}_{15}, \boldsymbol{x}_5\}, & \chi_6 &:= \{\boldsymbol{x}_8, \boldsymbol{x}_9, \boldsymbol{x}_{11}, \boldsymbol{x}_{13}, \boldsymbol{x}_{15}\}, \\
\chi_7 &:= \{\boldsymbol{x}_7, \boldsymbol{x}_9, \boldsymbol{x}_{10}, \boldsymbol{x}_{13}, \boldsymbol{x}_{14}\}, & \chi_8 &:= \{\boldsymbol{x}_7, \boldsymbol{x}_8, \boldsymbol{x}_9, \boldsymbol{x}_{10}, \boldsymbol{x}_{13}\}, \\
\chi_9 &:= \{\boldsymbol{x}_9, \boldsymbol{x}_{10}, \boldsymbol{x}_{13}, \boldsymbol{x}_{14}, \boldsymbol{x}_{15}\}, & \chi_{10} &:= \{\boldsymbol{x}_6, \boldsymbol{x}_9, \boldsymbol{x}_{10}, \boldsymbol{x}_{11}, \boldsymbol{x}_{12}\}, \\
\chi_{11} &:= \{\boldsymbol{x}_6, \boldsymbol{x}_8, \boldsymbol{x}_9, \boldsymbol{x}_{10}, \boldsymbol{x}_{11}\}, & \chi_{12} &:= \{\boldsymbol{x}_9, \boldsymbol{x}_{10}, \boldsymbol{x}_{11}, \boldsymbol{x}_{12}, \boldsymbol{x}_{15}\}, \\
\chi_{13} &:= \{\boldsymbol{x}_6, \boldsymbol{x}_7, \boldsymbol{x}_8, \boldsymbol{x}_9, \boldsymbol{x}_{10}\}, & \chi_{14} &:= \{\boldsymbol{x}_9, \boldsymbol{x}_{10}, \boldsymbol{x}_{12}, \boldsymbol{x}_{14}, \boldsymbol{x}_{15}\}, \\
\chi_{15} &:= \{\boldsymbol{x}_9, \boldsymbol{x}_{10}, \boldsymbol{x}_{11}, \boldsymbol{x}_{13}, \boldsymbol{x}_{15}\}, & \chi_{16} &:= \{\boldsymbol{x}_8, \boldsymbol{x}_9, \boldsymbol{x}_{10}, \boldsymbol{x}_{11}, \boldsymbol{x}_{13}\}.
\end{aligned}$$

The connectivity graph of this non–cyclic decomposition is shown in Fig. 11. We observe that the two pentatopes τ_{15} and τ_{16} share four interior tetrahedra and one boundary tetrahedron. The pentatopes $\tau_6, \ldots, \tau_{14}$ share three interior tetrahedra and two boundary tetrahedra. Thus all pentatopes have at least one boundary tetrahedron in common. As for the cyclic decomposition, it is possible to construct all pentatopes, all interior tetrahedra, and all boundary tetrahedra by using the connectivity graph as shown in Fig. 11.

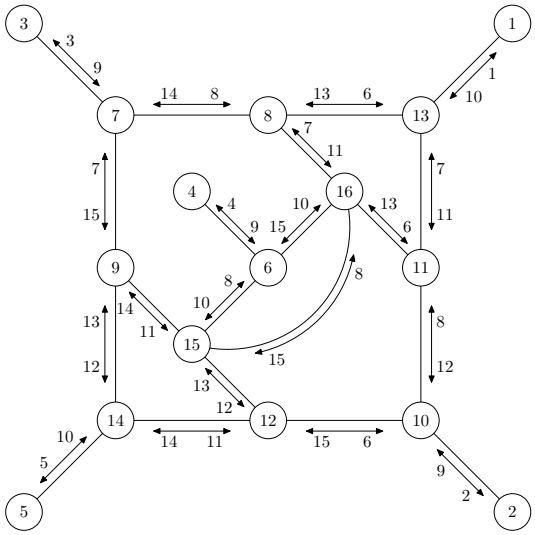

Figure 11: Connectivity graph of a non–cyclic decomposition of a pentatope.

3.3 Decomposing a hypercube

In this section we consider one possible decomposition of a hypercube $W_4 = [0,1]^4$ into 96 pentatopes. In [4], decompositions of a general hypercube $W_n = [0,1]^n$ are considered, and in [13, 17], decompositions of the hypercube W_4 into $N \leq 4! = 24$ pentatopes are presented. Here we will use the projection of the hypercube W_4 as shown in Fig. 12.
We first note that the n–dimensional cube W_n has $N_{W_{n-1}} = 2n$ $(n-1)$–dimensional cubes as surface, see, e.g., [9]. Hence, the hypercube W_4 has $N_{W_3} = 8$ cubes W_3^i, $i = 1, \ldots, 8$, as surface, see also the projection of the hypercube W_4 as shown in Figure 12. Moreover, every cube W_3^i consists of $N_{W_3} = 6$ squares $W_2^{i,j}$, $i = 1, \ldots, 8$, $j = 1, \ldots, 6$. If we use the midpoint $\boldsymbol{M} = (0.5, 0.5, 0.5, 0.5)^\top$ of the hypercube W_4, we can decompose the hypercube into 96 pentatopes τ_k. To do so, we use the midpoints $\boldsymbol{M}_i$ of the boundary cubes $W_3^i, i = 1, \ldots, 8$. We also decompose every square $W_2^{i,j}$ of a boundary cube W_3^i into two triangles. If we now use the three nodes of one of these triangles with the midpoint $\boldsymbol{M}_i$ of the boundary cube W_3^i, and the midpoint $\boldsymbol{M}$ of the hypercube, we have five nodes which form a pentatope τ_k, see also Fig. 12. Thus, the resulting decomposition consists of

$$N = 2N_{W_2}N_{W_3} = 96$$

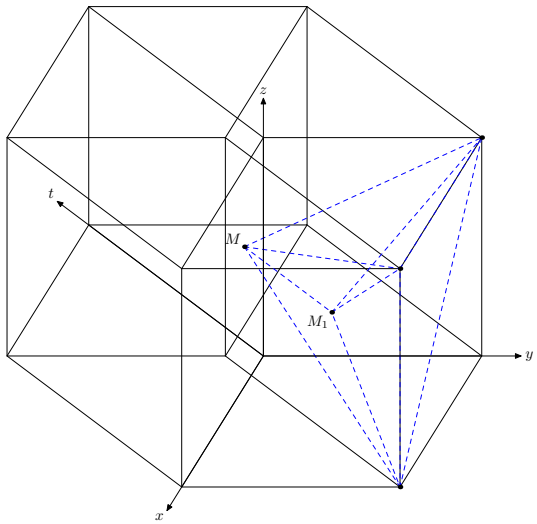

Figure 12: Decomposing a hypercube.

pentatopes τ_k of the same size.

3.4 Uniform refinement

In this section we present an algorithm to refine a given triangulation $\mathcal{T}_N$ uniformly. In Section 3.2 we treated the decomposition of a single pentatope $\tau_k \in \mathcal{T}_N$. In this case, we need to have either a cyclic or a non–cyclic fixing ϕ_k to do a refinement of τ_k into 16 smaller pentatopes. In the general case of two neighbouring pentatopes $\tau_k, \tau_\ell \in \mathcal{T}_N$ we have to choose the same interior edge of the joint tetrahedron to guarantee an admissible decomposition. This motivates the following definition.

Definition 3.12 (Admissible fixing) *Let $\mathcal{T}_N$ be an admissible deomposition. Two neighbouring pentatopes $\tau_k, \tau_\ell \in \mathcal{T}_N$ are fixed admissibly, if the fixed edge $e_{k\ell}$ of the joint tetrahedron satisfies*

$$e_{k\ell} \in \phi_k \cap \phi_\ell,$$

where ϕ_k and ϕ_ℓ are cyclic or non–cyclic fixings of the pentatopes τ_k and τ_ℓ, respectively. A decomposition $\mathcal{T}_N$ is called admissible fixed, if all neighbouring pentatopes of the decomposition $\mathcal{T}_N$ are admissible fixed.

If a decomposition $\mathcal{T}_N$ is admissible fixed, then the application of the decompositions as given in Definitions 3.10 and 3.11 result in an admissible decomposition $\mathcal{T}_{16N}$. An algorithm to obtain an admissible fixing for all pentatopes is given in Algorithm 13 where the smallest interior edges are used to fix the pentatopes $\tau_k \in \mathcal{T}_N$.
In Tables 1–3 the main properties of a uniform decomposition of a pentatope and of a hypercube are presented, where for each level we give the number of pentatops, the number

For $k = 1, 2, \ldots, N$:

For all tetrahedrons $\sigma_{k,i}$ of the pentatope $\tau_k \in \mathcal{T}_N$ do:

For $i = 1, \ldots, 5$:

Derive the interior edges $\Phi_{k,i}$.

Calculate the smallest interior edge of the tetrahedron $\sigma_{k,i}$

$$e_{k,i} := \arg \min_{e_n \in \Phi_{k,i}} |e_n| .$$

Further determine the set

$$A_{k,i} := \{e_n \in \Phi_{k,i} : |e_n| = |e_{k,i}|\}.$$

If $|A_{k,i}| = 1$, then fix the edge $e_{k,i}$ of the tetrahedron $\sigma_{k,i}$.

EndFor

EndFor

For $k = 1, 2, \ldots, N$:

For $i = 1, \ldots, 5$:

If the tetrahedron $\sigma_{k,i}$ of the pentatope $\tau_k \in \mathcal{T}_N$ is not fixed, then fix an appropriate edge $e \in A_{k,i}$.

EndFor

EndFor

For $k = 1, 2, \ldots, N$:

If the fixing ϕ_k of the pentatope τ_k is not connected, then change an appropriate edge of the fixing ϕ_k.

EndFor

Algorithm 13: Fixing all pentatopes τ_k of a triangulation $\mathcal{T}_N$.

of boundary and interior tetrahedra, the number of nodes, the maximal mesh size, and the maximal diameter. Note that for the hypercube two different initial decompositions with $N = 96$ and $N = 24$ pentatopes are used.

level	elements	boundary elements	interior elements	nodes	$h_{\max}$	$\max_{k=1,\dots,N} d_k$
1	1	5	0	5	0.4518	1.4142
2	16	40	20	15	0.2259	1.0000
3	256	320	480	70	0.1130	0.5590
4	4096	2560	8960	495	0.05648	0.2795
5	65536	20480	153600	4845	0.02824	0.1531
6	1048576	163840	2539520	58905	0.01412	0.07655

Table 1: Decomposition of a pentatope.

level	elements	boundary elements	interior elements	nodes	$h_{\max}$	$\max_{k=1,\dots,N} d_k$
1	96	96	192	25	0.3195	1.4142
2	1536	768	3456	169	0.1597	0.7071
3	24576	6144	58368	1681	0.07987	0.3750
4	393216	49152	958464	21025	0.03994	0.1875
5	6291456	393216	15532032	297025	0.01997	0.1083
6	100663296	3145728	250085376	4464769	0.009984	0.05634

Table 2: Decomposition of a hypercube (96 initial elements).

level	elements	boundary elements	interior elements	nodes	$h_{\max}$	$\max_{k=1,\dots,N} d_k$
1	24	48	36	16	0.4518	2.0000
2	384	384	768	81	0.2259	1.1180
3	6144	3072	13824	625	0.1130	0.5590
4	98304	24576	233472	6561	0.05648	0.3062
5	1572864	196608	3833856	83521	0.02824	0.1531
6	25165824	1572864	1572864	1185921	0.01412	0.08268

Table 3: Decomposition of a hypercube (24 initial elements).

It is also possible to use the particular cyclic fixing

$$\phi = \{(\boldsymbol{x}_{11}, \boldsymbol{x}_{14}), (\boldsymbol{x}_8, \boldsymbol{x}_{14}), (\boldsymbol{x}_8, \boldsymbol{x}_{12}), (\boldsymbol{x}_7, \boldsymbol{x}_{12}), (\boldsymbol{x}_7, \boldsymbol{x}_{11})\}$$

for the decomposition of all pentatopes $\tau_k \in \mathcal{T}_N$. This special decomposition can be applied recursively to all pentatopes of $\mathcal{T}_N$ to get a uniform refinement. The resulting node numbers

are given in Table 4. To guarantee an admissible decomposition, the nodes of the initial decomposition have to be sorted in the right way, see Definition 3.13. This approach is equivalent to the global application of the Freudenthal algorithm [6, 11, 12]. In Tables 5–7 the main properties are given for the case of an uniform refinement by using only one particular cyclic decomposition. We observe that the maximal diameter $\max d_k$ of all pentatops $\tau_k \in \mathcal{T}_N$ reduces by a factor of two for each level $\ell > 1$, which was proved by Bey [6].

1	1	6	7	8	9
2	6	2	10	11	12
3	7	10	3	13	14
4	8	11	13	4	15
5	9	12	14	15	5
6	7	8	11	12	14
7	8	11	13	14	15
8	8	11	12	14	15
9	7	10	11	12	14
10	7	10	11	13	14
11	8	9	12	14	15
12	7	8	9	12	14
13	7	8	11	13	14
14	6	7	8	9	12
15	6	7	8	11	12
16	6	7	10	11	12

Table 4: Node numbers of the special cyclic decomposition of a pentatope.

level	elements	boundary elements	interior elements	nodes	$h_{\max}$	$\max\limits_{k=1,\ldots,N} d_k$
1	1	5	0	5	0.4518	1.4142
2	16	40	20	15	0.2259	1.0000
3	256	320	480	70	0.1130	0.5000
4	4096	2560	8960	495	0.05648	0.2500
5	65536	20480	153600	4845	0.02824	0.1250
6	1048576	163840	2539520	58905	0.01412	0.0625

Table 5: Cyclic decomposition of a pentatope.

Definition 3.13 (Consistently numbered) *A decomposition $\mathcal{T}_N$ is called consistently numbered, if for two pentatopes*

$$\tau_k = \operatorname{conv}(\{x_1, \ldots, x_5\}), \tau_\ell = \operatorname{conv}(\{y_1, \ldots, y_5\}) \in \mathcal{T}_N$$

level	elements	boundary elements	interior elements	nodes	$h_{\max}$	$\max_{k=1,\ldots,N} d_k$
1	96	96	192	25	0.3195	1.4142
2	1536	768	3456	169	0.1597	0.8660
3	24576	6144	58368	1681	0.07987	0.4330
4	393216	49152	958464	21025	0.03994	0.2165
5	6291456	393216	15532032	297025	0.01997	0.1083
6	100663296	3145728	250085376	4464769	0.009984	0.05413

Table 6: Cyclic decomposition of a hypercube (96 initial elements).

level	elements	boundary elements	interior elements	nodes	$h_{\max}$	$\max_{k=1,\ldots,N} d_k$
1	24	48	36	16	0.4518	2.0000
2	384	384	768	81	0.2259	1.5000
3	6144	3072	13824	625	0.1130	0.7500
4	98304	24576	233472	6561	0.05648	0.3750
5	1572864	196608	3833856	83521	0.02824	0.1875
6	25165824	1572864	62128128	1185921	0.01412	0.09375

Table 7: Cyclic decomposition of a hypercube (24 initial elements).

there exist indices $i_1 < i_2 < \ldots < i_\ell$ *and* $j_1 < j_2 < \ldots < j_\ell$ *with* $1 \leq \ell \leq 5$ *such that*

$$\{x_1, \ldots, x_5\} \cap \{y_1, \ldots, y_5\} \cong \{x_{i_1}, x_{i_2}, \ldots, x_{i_\ell}\} \equiv \{y_{j_1}, y_{j_2}, \ldots, y_{j_\ell}\}.$$

The symbol $\cong$ *means that two sets are isomorphic to each other, and the symbol* $\equiv$ *means, that two sets are equal and the order of the elements is the same.*

If the node numbers of the pentatopes $\tau_k \in \mathcal{T}_N$ are sorted by their global node numbers, then it follows easily that the decomposition is consistently numbered.

3.5 Visualization

We finally present an algorithm to visualize a four–dimensional decomposition $\mathcal{T}_N$. The idea is to cut the decomposition into a finite number of three–dimensional manifolds. For this we need to have a hyperplane to calculate the intersections with the decomposition.

Definition 3.14 (Hyperplane) *Let* $\boldsymbol{P}_0 \in \mathbb{R}^4$ *be arbitrary, and* $\boldsymbol{P}_1, \boldsymbol{P}_2, \boldsymbol{P}_3 \in \mathbb{R}^4$ *are assumed to be linear independent vectors. Then the set*

$$E_4 := \{x : x = \boldsymbol{P}_0 + \mu_1 \boldsymbol{P}_1 + \mu_2 \boldsymbol{P}_2 + \mu_3 \boldsymbol{P}_3 \quad \textit{for} \quad \mu_1, \mu_2, \mu_3 \in \mathbb{R}\}$$

describes a hyperplane.

To cut a given decomposition $\mathcal{T}_N$ with a hyperplane, we have to cut every pentatope $\tau_k \in \mathcal{T}_N$ with the hyperplane. For this we have to calculate for every edge $e_i = (\boldsymbol{x}_{i_1}, \boldsymbol{x}_{i_2})$, $i = 1, \ldots, 10$, of a pentatope τ_k the intersection with the hyperplane. A point $\boldsymbol{x} \in e_i$ can be written as

$$\boldsymbol{x} = \boldsymbol{x}_{i_1} + \lambda(\boldsymbol{x}_{i_2} - \boldsymbol{x}_{i_1}) \quad \text{for } \lambda \in [0, 1].$$

Thus an intersection point $\boldsymbol{x}_i$ of the edge e_i with a hyperplane E_4 has to satisfy the equation

$$\boldsymbol{x}_{i_1} + \lambda(\boldsymbol{x}_{i_2} - \boldsymbol{x}_{i_1}) = \boldsymbol{P}_0 + \mu_1 \boldsymbol{P}_1 + \mu_2 \boldsymbol{P}_2 + \mu_3 \boldsymbol{P}_3$$

which is equivalent to the system of linear equaions

$$\underbrace{\begin{pmatrix} \boldsymbol{P}_1 & \boldsymbol{P}_2 & \boldsymbol{P}_3 & \boldsymbol{x}_{i_1} - \boldsymbol{x}_{i_2} \end{pmatrix}}_{=:A_i} \begin{pmatrix} \mu_1 \\ \mu_2 \\ \mu_3 \\ \lambda \end{pmatrix} = \left(\boldsymbol{x}_{i_1} - \boldsymbol{P}_0 \right). \tag{3.3}$$

The matrix A_i is invertible if and only if the vector $\boldsymbol{x}_{i_1} - \boldsymbol{x}_{i_2}$ is linear independent to the vectors $\boldsymbol{P}_1$, $\boldsymbol{P}_2$ and $\boldsymbol{P}_3$. In fact, the matrix A_i is not invertible if the edge e_i is parallel to the hyperplane E_4. In this case there exists either no intersection point or infinitly many intersection points of the edge e_i with the hyperplane. If the matrix is invertible we can calculate the coefficients $\mu_1, \mu_2, \mu_3, \lambda \in \mathbb{R}$ uniquely. For $\lambda \in [0, 1]$,

$$\boldsymbol{x}_i = \boldsymbol{x}_{i,1} + \lambda(\boldsymbol{x}_{i,2} - \boldsymbol{x}_{i,1}) = \boldsymbol{P}_0 + \mu_1 \boldsymbol{P}_1 + \mu_2 \boldsymbol{P}_2 + \mu_3 \boldsymbol{P}_3$$

is an intersection point of the edge e_i with the hyperplane E_4. The set D_k denotes all intersection points of the pentatope τ_k with the hyperplane E_4. There are three interesting cases:

i. If $|D_k| = 4$, then the intersection points form a tetrahedron.

ii. For $|D_k| = 6$ we get in general an irregular prisma.

iii. If $|D_k| \leq 3$, then the intersection points of D_k are not relevant for the visualization.

If we use the vectors

$$\boldsymbol{P}_0 = (0, 0, 0, t)^\top, \boldsymbol{P}_1 = (1, 0, 0, 0)^\top, \boldsymbol{P}_2 = (0, 1, 0, 0)^\top \text{ and } \boldsymbol{P}_3 = (0, 0, 1, 0)^\top$$

to describe a hyperplane $E_4(t)$ at a given time $t \in [0, T]$, we can calculate for every time t a three–dimensional object which can be visualized with the usual methods, see, e.g., [14].

4 Numerical results

As a first numerical example we consider the transient heat equation (2.1) with the boundary conditions (2.2) and with the initial conditions (2.3) for the particular case $\Omega = (0,1)^3 \subset \mathbb{R}^3$ and $T = 1$. The functions $f(\boldsymbol{x},t)$ and $u_0(\boldsymbol{x})$ are chosen such that

$$u(\boldsymbol{x},t) = \sin(\pi x_1)\sin(\pi x_2)\sin(\pi x_3)(1-t)^2$$

is the exact solution which is sufficient regular. For the meshing of the space time cylinder $Q = (0,1)^4 \subset \mathbb{R}^4$ we use the uniform triangulations as given in Table 6. For the computation of the approximate solutions we use the discontinuous Galerkin finite element method with piecewise linear basis functions as described in Chapter 2. In Table 4 we give the $L_2(Q)$–errors of the approximate solutions which are computed with respect to different refinement levels. As predicted by the theory, see the error estimate (2.5), we observe an estimated order of convergence (eoc) of 2.

level	elements	dof	$\|u-u_h\|_{L_2(Q)}$	eoc
0	96	120	$6.3903-2$	–
1	1536	3546	$4.6208-2$	0.47
2	24576	83155	$1.2104-2$	1.93
3	393216	1620793	$2.8615-3$	2.08
4	6291456	28587985	$6.7072-4$	2.09

Table 8: Numerical results for $p = 1, \sigma = 10, \beta = 1, \varepsilon = -1$.

As a second example of more practical interest we consider the simulation of a pump in two space dimensions, see Fig. 14. The rotor rotates with an angular speed ω and therefore the fluid domain Ω also depends on time. The fluid is modelled by the transient Navier–Stokes equations with a viscosity of $\nu = 1$. The angular velocity of the rotor is $\omega = 0.1$, the inflow and outflow boundary conditions for the boundary stress at Σ_N are set to zero, and the velocity at the remaining boundary is also zero. In addition, we assume as initial condition $\boldsymbol{u}_0(\boldsymbol{x}) = 0$ for $\boldsymbol{x} \in \Omega$. In Fig. 15–17 we present the absolute values of the calculated velocity at several times.

The main advantage of the proposed approach may consist in a flexible handling of adaptive meshes in space and time. To illustrate this, we consider the heat equation (2.1) for $\Omega = (0,1)$, i.e. $n = 1$, and $T = 1$, where the exact solution is given by

$$u(x,t) = e^{-2(2+5t-10x)^2}.$$

For the space time cylinder $Q = (0,1)^2$ we use the adaptive mesh as shown in Fig. 18. The approximate solution is computed by the discontinuous Galerkin finite element method where the parameters are chosen to be $p = 1$, $\beta = 1$, and $\varepsilon = -1$. In the adaptive case we end up with 5741 degrees of freedom, while a comparable uniform refinement would result in 24320 degrees of freedom.

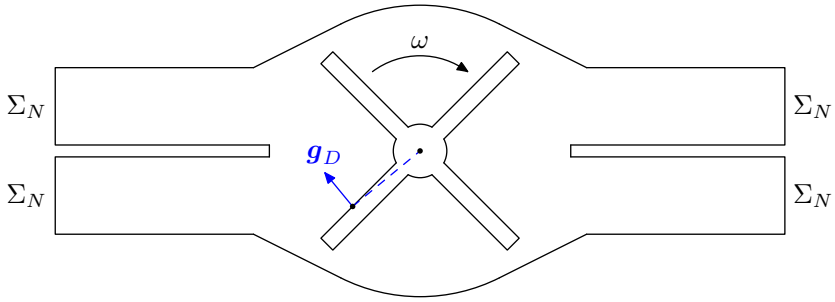

Figure 14: Domain $\Omega(t)$.

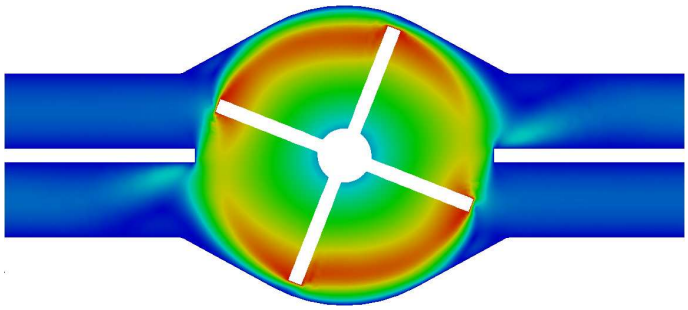

Figure 15: Pump simulation at $t = 0.625$.

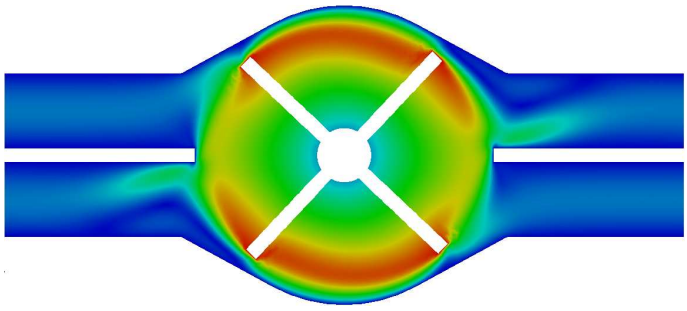

Figure 16: Pump simulation at $t = 1.25$.

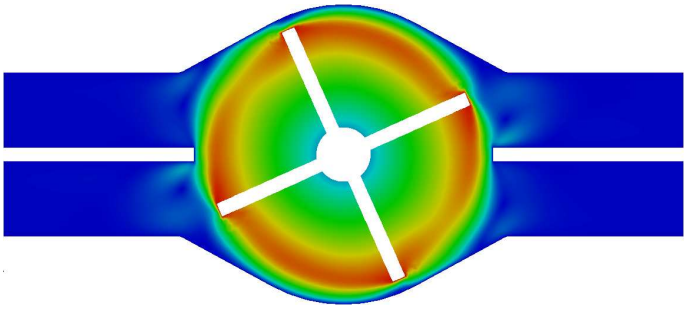

Figure 17: Pump simulation at $t = 1.875$.

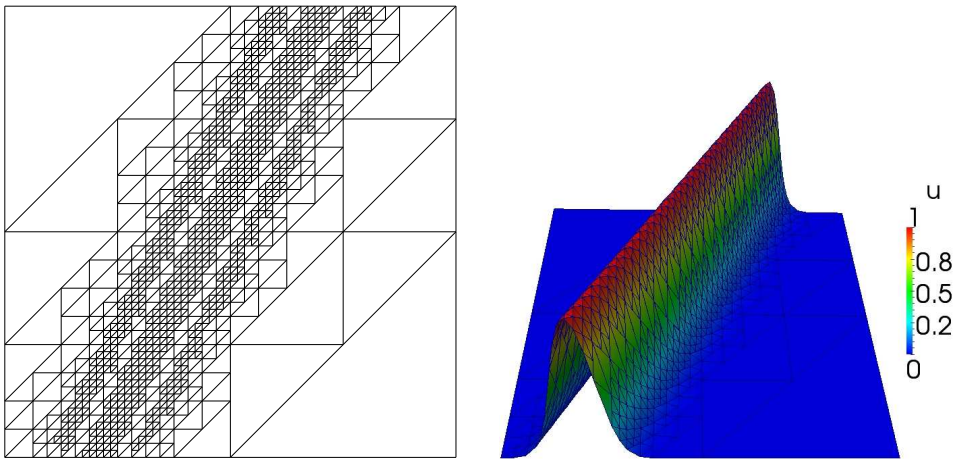

Figure 18: Adaptive space–time mesh and approximate solution u_h.

5 Conclusions

In this paper we have presented a discontinuous Galerkin finite element method which is applicable to deal with flexible meshes in space and time. This approach relies on suitable decompositions in space and time. In particular for three–dimensional objects we have presented a refinement strategy to construct finite element meshes consisting of pentatopes. While for one– or two–dimensional spatial domains we may use standard tools to mesh the space time cylinder in two or three dimensions, respectively, we only considered the particular case of the unit cube in three space dimensions. However, an initial mesh for arbitrary domains $\Omega \subset \mathbb{R}^3$ can be constructed by using a standard uniform time discretization, and using adaptive refinement strategies afterwards. For this we need to formulate and to analyse appropriate a posteriori error estimatores, as used, for example, in advection–diffusion problems with nonnegative characteristic forms. For the iterative solution of the resulting algebraic systems of linear equations we may consider domain decomposition methods, i.e., we may introduce Langrange multiplier on the interface to obtain a hybrid formulation, see, e.g., [8, 10].

Acknowledgement

This work was supported by the Austrian Science Fund (FWF) within the SFB Mathematical Optimization and Applications in Biomedical Sciences.

References

[1] R. Abedi, S.–H. Chung, J. Erickson, Y. Fan, M. Garland, D. Guoy, R. Haber, J. M. Sullivan, S. Thite, Y. Zhou: Spacetime meshing with adaptive refinement and coarsening. In: Proceedings of Symposium on Computational Geometry, pp. 300–309, 2004.

[2] D. N. Arnold, F. Brezzi, B. Cockburn, D. Marini: Unified analysis of discontinuous Galerkin methods for elliptic problems. SIAM J. Numer. Anal. 39 (2002) 1749–1779.

[3] C. E. Baumann, J. T. Oden: A discontinuous hp finite element method for convection–diffusion problems. Comput. Methods Appl. Mech. Engrg. 175 (1999) 311–341.

[4] L. Baumgartner: Zerlegung des n–dimensionalen Raumes in kongruente Simplexe. Math. Nachr. 48 (1971) 213–224.

[5] M. Behr: Simplex space–time meshes in finite element simulations. Internat. J. Numer. Methods Fluids 57 (2008) 1421–1434.

[6] J. Bey: Simplicial grid refinement on Freudenthal's algorithm and the optimal number of congruence classes. Numer. Math. 85 (2000) 1–29.

[7] Z. Chen, H. Steeb, S. Diebels: A space–time discontinuous Galerkin method applied to single–phase flow in porous media. Comput. Geosci. 12 (2008) 525–539.

[8] B. Cockburn, J. Gopalakrishnan, R. Lazarov: Unified hybridization of discontinuous Galerkin, mixed, and continuous Galerkin methods for second order elliptic problems. SIAM J. Numer. Anal. 47 (2009) 1319–1365.

[9] H. S. M. Coxeter: Regular Polytopes. Dover, New York, 1973.

[10] H. Egger, J. Schöberl: A hybrid mixed discontinuous Galerkin finite–element method for convection–diffusion problems. IMA J. Numer. Anal. 30 (2010) 1206–1234.

[11] H. Freudenthal: Simplizialzerlegungen von beschränkter Flachheit. Ann. Math. 43 (1942) 580–582.

[12] E. N. Gonçalves, R. M. Palhares, R. H. C. Takahashi, R. C. Mesquita: Algorithm 860: SimpleS – an extension of Freudenthal's simplex subdivision. ACM Trans. Math. Software 32 (2006) 609–621.

[13] M. Haiman: A simple and relatively efficient triangulation of the n–cube. Discrete Comput. Geom. 6 (1991) 287–289.

[14] C. R. Johnson, C. Hansen: The Visualization Handbook. Elsevier–Butterworth Heinemann, Oxford, 2005.

[15] A. Masud, T. J. R. Hughes: A space–time Galerkin/least–squares finite element formulation of the Navier–Stokes equations for moving domain problems. Comput. Methods Appl. Mech. Engrg. 146 (1997) 91–126.

[16] M. Neumüller: Eine Finite Element Methode für optimale Kontrollprobleme mit parabolischen Randwertaufgaben. Masterarbeit, Institut für Numerische Mathematik, Technische Universität Graz, 2010.

[17] D. Orden: Asymptotically efficient triangulations of the d–cube. Discrete Comput. Geom. 30 (2003) 509–528.

[18] B. Rivière: Discontinuous Galerkin Methods for Solving Elliptic and Parabolic Equations. SIAM, Philadelphia, 2008.

[19] J. J. Sudirham, J. J. W. van der Vegt, R. M. J. van Damme: Space–time discontinuous Galerkin method for advection–diffusion problems on time–dependent domains. Appl. Numer. Math. 56 (2006) 1491–1518.

[20] T. E. Tezduyar: Interface–tracking and interface–capturing techniques for finite element computation of moving boundaries and interfaces. Comput. Methods Appl. Mech. Engrg. 195 (2006) 2983–3000.

[21] T. E. Tezduyar, M. Behr, J. Liou: A new strategy for finite element computations involving moving boundaries and interfaces – the deforming–spatial–domain/space–time procedure. I. The concept and the preliminary numerical tests. Comput. Methods Appl. Mech. Engrg. 94 (1992) 339–351.

[22] T. E. Tezduyar, M. Behr, S. Mittal, J. Liou: A new strategy for finite element computations involving moving boundaries and interfaces – the deforming–spatial–domain/space–time procedure. II. Computation of free–surface flows, two–liquid flows, and flows with drifting cylinders. Comput. Methods Appl. Mech. Engrg. 94 (1992) 353–371.

[23] T. E. Tezduyar, S. Sathe: Enhanced–discretization space–time technique (EDSTT). Comput. Methods Appl. Mech. Engrg. 193 (2004) 1385–1401.

[24] V. Thomee: Galerkin Finite Element Methods for Parabolic Problems. Springer, Berlin-Heidelberg, 1997.

[25] J. J. W. van der Vegt, J. J. Sudirham: A space–time discontinuous Galerkin method for the time–dependent Oseen equations. Appl. Numer. Math. 58 (2008) 1892–1917.

Appendix

In this appendix we present all possible connected fixings. Out of the 243 possible sets of fixed edges, there are 87 different connected fixings. The 87 connected fixings are splitted up in 12 cyclic fixings and 75 non–cyclic fixings.

Cyclic fixings

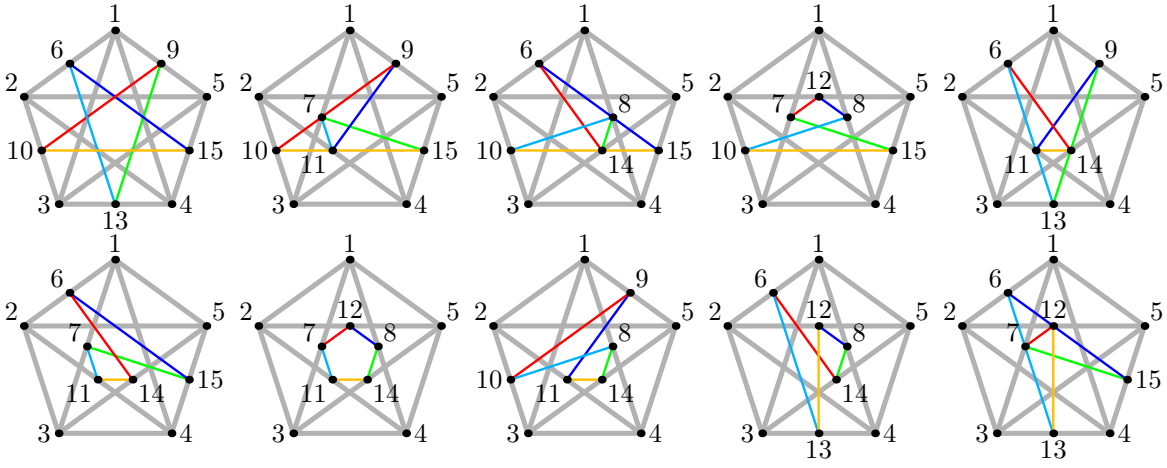

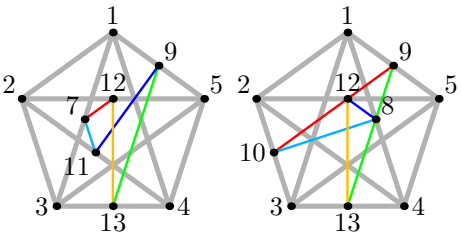

Non-cyclic fixings

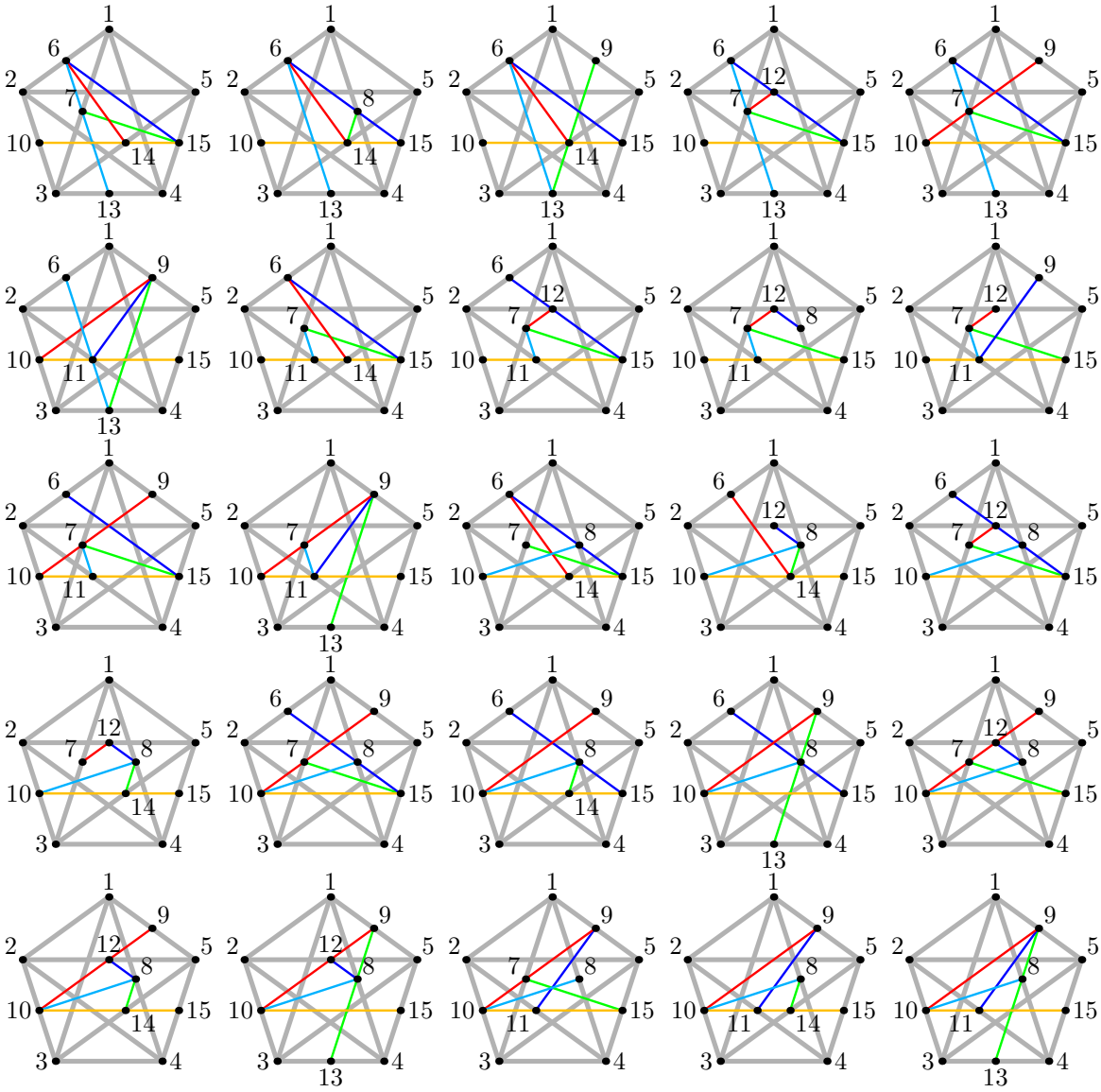

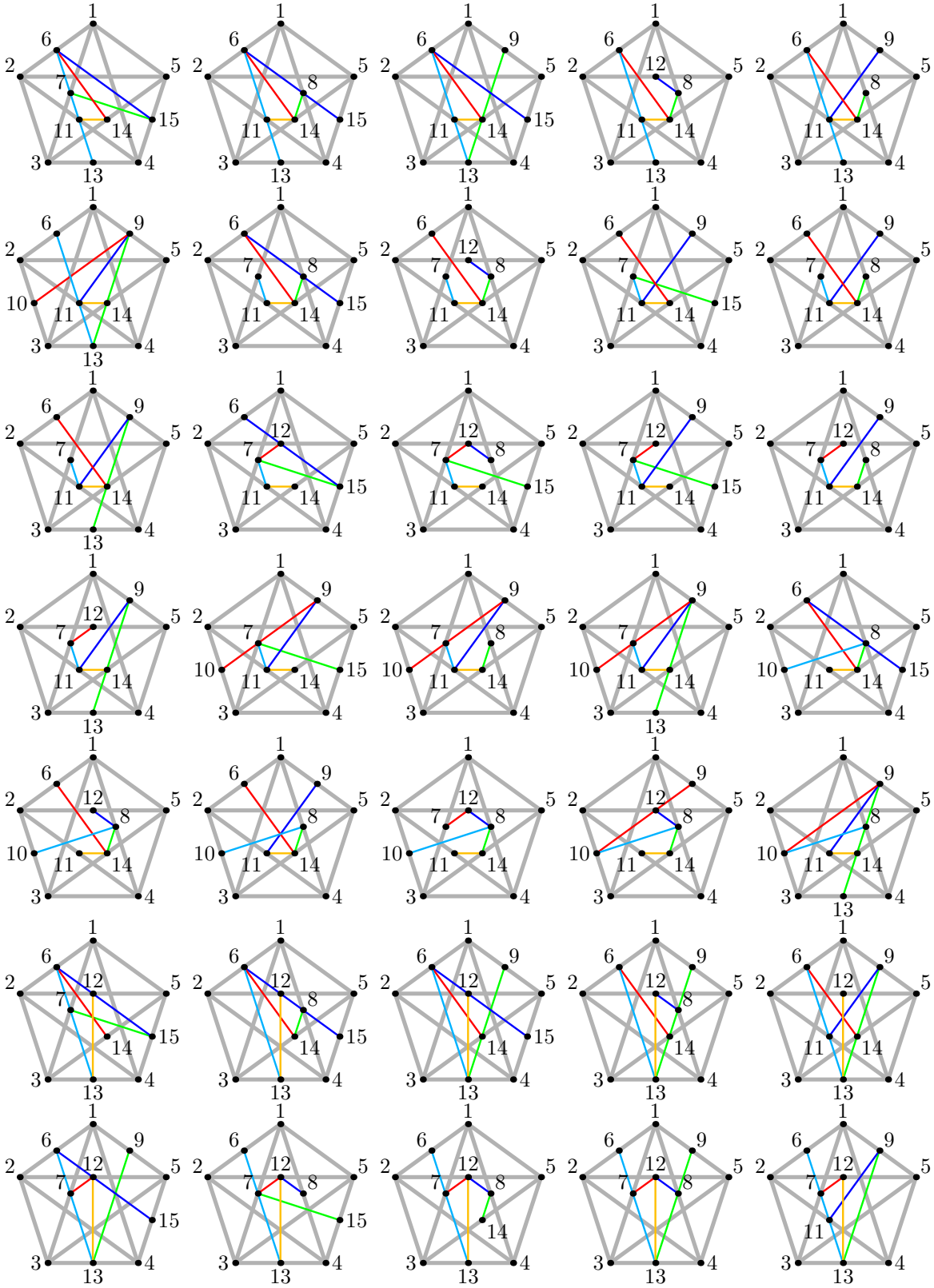

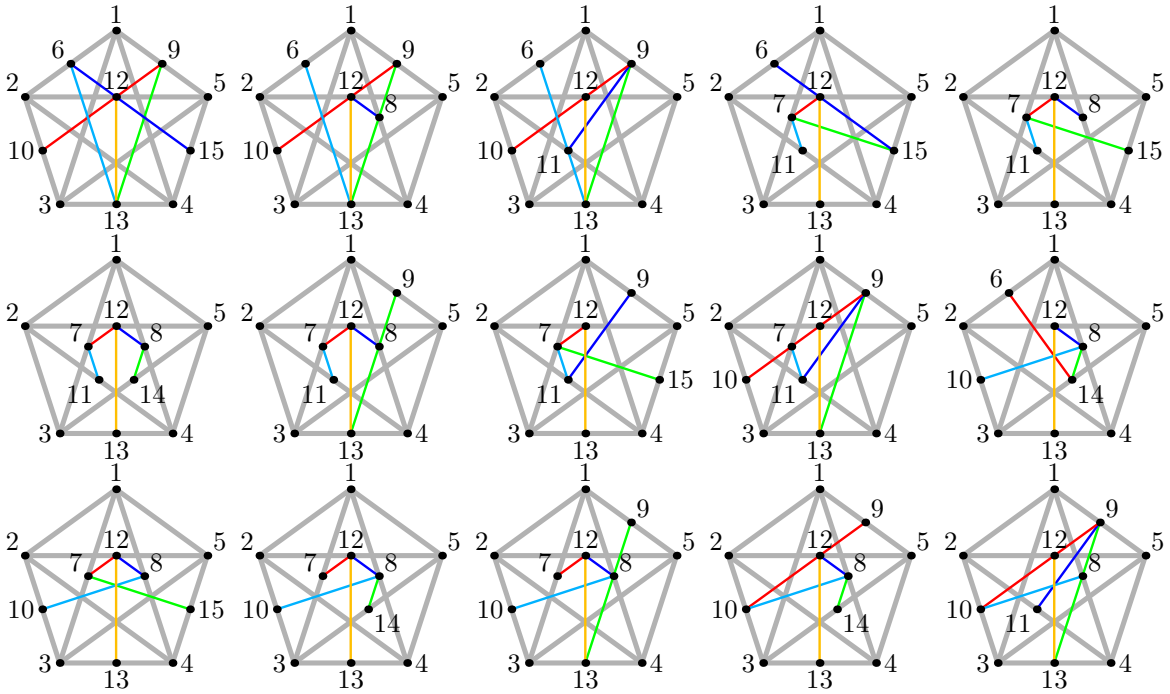
1 6 9 2 12 5 10 15 3 13 4
1 6 9 2 12 8 5 10 3 13 4
1 6 9 2 12 5 11 10 3 13 4
1 6 9 2 12 5 7 11 15 3 13 4
1 12 5 7 8 11 15 3 13 4
1 12 5 7 8 11 14 3 13 4
1 9 2 12 5 7 8 11 3 13 4
1 9 2 12 5 7 15 11 3 13 4
1 9 2 12 5 7 8 10 11 3 13 4
1 6 12 5 8 10 14 3 13 4
1 12 5 7 8 10 15 3 13 4
1 12 5 7 8 10 14 3 13 4
1 9 2 12 5 7 8 10 3 13 4
1 9 2 12 5 8 10 14 3 13 4
1 9 12 5 8 10 11 3 13 4